Dynamic m^{6}A methylation facilitates mRNA triaging to stress granules

Maximilian Anders,[1,3] Irina Chelysheva,[1,3] Ingrid Goebel,[1] Timo Trenkner,[1] Jun Zhou,[2] Yuanhui Mao,[2] Silvia Verzini,[1] Shu-Bing Qian,[2] and Zoya Ignatova[1,*]

[1]Biochemistry and Molecular Biology, Department of Chemistry, University of Hamburg, 20146 Hamburg, Germany
[2]Division of Nutritional Sci., Cornell Univ., Ithaca, NY, 14853, USA
[3]These authors contributed equally

*Corresponding author. Tel: +49 40 42838 2332; E-mail: zoya.ignatova@uni-hamburg.de

Summary blurb

m^{6}A-modification in the 5' vicinity of the coding sequence of transcripts provides a selective mechanism for triaging mRNAs to stress granules and is mediated by YTHDF3 'reader' protein.

Abstract

Reversible post-transcriptional modifications on messenger RNA emerge as prevalent phenomena in RNA metabolism. The most abundant among them is N^6-methyladenosine (m^{6}A) which is pivotal for RNA metabolism and function, its role in stress response remains elusive. We have discovered that in response to oxidative stress, transcripts are additionally m^{6}A-modified in their 5' vicinity. Distinct from that of the translationally-active mRNAs, this methylation pattern provides a selective mechanism for triaging mRNAs from the translatable pool to stress-induced stress granules. These stress-induced newly methylated sites are selectively recognized by the YTH domain family 3 (YTHDF3) 'reader' protein, thereby revealing a new role for YTHDF3 in shaping the selectivity of stress response. Our findings describe a previously unappreciated function for RNA m^{6}A modification in the oxidative-stress response and expand the breadth of physiological roles of m^{6}A.

Introduction

Adequate reprogramming of metabolic activities by environmental stress or suboptimal growth conditions is crucial for cell survival. In eukaryotes, the most potent stress-induced inhibition of translation is repression of translational initiation by kinases-induced phosphorylation of Ser51 of eIF2α, which selectively represses translation of mRNAs with cap-dependent translation (Sonenberg & Hinnebusch, 2009). Translationally-stalled mRNAs are deposited in stress granules (SG), membraneless RNA-protein particles (RNPs) that along with non-translating mRNAs associated with translation initiation complexes contain RNA-binding proteins and proteins with low complexity or intrinsically disordered regions (IDRs) (Buchan & Parker, 2009; Jain et al, 2016; Kedersha et al, 2013; Protter & Parker, 2016). SGs are dynamic structures whose assembly is modulated by protein-protein interactions frequently involving their IDRs while translationally stalled mRNAs serve as scaffolds for attachment of the RNA-binding proteins (Panas et al, 2016; Protter & Parker, 2016). SGs are heterogeneous in structure, with denser parts (termed cores) linked by less concentrated regions (termed shells) (Protter & Parker, 2016). In mammalian cells, quantification of the RNA constituents of the SG cores by RNA-sequencing (RNA-Seq) revealed that the targeting efficiency for different mRNAs largely varies and a relatively small fraction of bulk mRNAs accumulates in them (Khong et al, 2017). While through such systemic approaches our knowledge of protein and mRNA components of the SG cores is steadily increasing (Jain et al, 2016; Khong et al, 2017), whether the composition of the shell differs from that of the core remains elusive.

A long-standing question is the mechanism by which cellular mRNAs are selected in SGs. A prevailing hypothesis has been that stress-induced stalling of cap-dependent initiation is a major sorting factor for triaging mRNAs into SGs which is consistent with their composition (Buchan & Parker, 2009; Kedersha et al, 2013; Sonenberg & Hinnebusch, 2009). SGs typically contain translating poly(A) mRNAs, 40S ribosomal subunit, different initiation factors and are sensitive to drugs that impair translation initiation, although the composition can vary dependent on the type of stress (Buchan & Parker, 2009; Kedersha et al, 2005; Protter & Parker, 2016). For example, initiation factors necessary for assembly of the preinitiation complex might be absent in SGs, arguing that not all mRNAs within SGs are stalled at initiation (Kedersha et al, 2005). Furthermore,

various types of stress inhibit translation downstream of initiation (Liu et al, 2013). Recent study reveals that mRNA clients of the mammalian SG cores are enriched in species with longer coding and UTR regions and suggests that inefficient translation and/or poor association with ribosomes facilitates association with RNA-binding proteins and consequently with SGs (Khong et al, 2017). However, the full population of mRNAs in SGs, including those from the more mobile periphery, and more specifically mechanistic details underlying mRNA selection and triaging to SGs have not been addressed.

Under various types of stress, a sizeable subset of genes escapes global kinase(s)-dependent inhibition of translation and remains translationally active and likely shapes the stress-dependent gene expression at the level of translation. Recently discovered mechanism of mRNA modification in 5'UTRs offers an attractive solution of this central conundrum: a prevalent methylation at position 6 of adenosine (m^6A) in the 5'UTRs enables cap-independent translation (Coots et al, 2017; Meyer et al, 2015; Zhou et al, 2015). m^6A is the most abundant post-transcriptional modification on mRNA (Roundtree et al, 2017) and is crucial for RNA metabolism, including RNA stability (Wang et al, 2014), splicing (Dominissini et al, 2012; Liu et al, 2015); miRNA processing (Alarcon et al, 2015a; Alarcon et al, 2015b), mediates translation under normal growth and heat stress (Meyer et al, 2015; Wang et al, 2015; Zhou et al, 2015) or facilitates repair of ultraviolet-induced DNA damage sites (Xiang et al, 2017). m^6A in mRNAs is reversibly installed at conserved sequences, e.g. the DRACH motif (D = A/G/U; R =A/G and H = U/A/C)(Meyer & Jaffrey, 2017) by the 'writer' complex (METTL3, METTL14 and WTAP) and reversed by demethylases termed 'erasers' (FTO, ALKBH5) (Roundtree et al, 2017). Under permissive growth, 3'UTRs exhibit the highest m^6A-modification levels, which mainly control mRNA stability (Meyer et al, 2012; Wang et al, 2014). The CDSs are the largest segments in mRNA and contain statistically the most DRACH motifs, however under physiological conditions they are poorly m^6A modified as compared to the 3'UTRs. This raises the fundamental questions: Are m^6A modifications in the CDSs dynamic and maybe stress-related? Do they contribute to the dynamics of SGs and play a role in selection of mRNAs in SGs?

Herein, combining systemic deep-sequencing-based approaches with single transcript analysis we investigated the dynamics of m^6A modification under mild (200 µM arsenite, AS) and severe (500 µM AS) oxidative stress in mammalian cells. We use cross-linking approach that stabilizes SGs and allows for isolation of the whole SG particles including their mobile shells. Along with mRNAs with stalled initiation complexes, which signals the SG association, in a large set of SG mRNA clients we detected a pervasive m^6A modification. Our results suggest a role of m^6A in selectively triaging mRNA to SGs.

Results

Oxidative stress induces additional methylation on mRNA

To dissect the dynamics of m^6A modification under oxidative stress, we took advantage of two different cells lines that stably express SG marker proteins, U2OS-G3BP1 (Ohn et al, 2008) and HEK-TIA1 (Damgaard & Lykke-Andersen, 2011). These SG marker proteins, G3BP1 and TIA1, are GFP or FLAG-tagged, respectively, which enables immuno(fluorescent) detection of SGs. To elicit oxidative stress, we used arsenite (AS). In both cell lines, SGs formed in a dose-dependent manner (Fig S1A) and contained both mRNAs and proteins (Fig S1B and Table S1) previously

identified in SGs (Jain et al, 2016; Khong et al, 2017). The maximal stress dose (500 µM AS) and exposure (30 min) we used, caused only marginal changes in the total mRNA levels as revealed by RNA-Seq (Fig. S1C). Overall, comparing to the total mRNAs detected under permissive growth (reads per kilobase per million reads (RPKM) over the spike-in threshold), we did detect only 6.5% decrease of the total mRNA under stress (Fig S1C), consistent with previous observations that short AS exposure does not trigger a global transcriptional response and alters the stability of few specific mRNAs (Andreev et al, 2015). Gene ontology (GO) enrichment analysis of the genes degraded under stress showed enriched categories (enrichment score 7.67) related to transcription (fold enrichment 1.94; $p = 7.88.10^{-8}$), including 'regulation of transcription' (fold enrichment 2.01; $p = 8.28.10^{-7}$), 'transcription factor activity' (fold enrichment 2.11; $p = 3.12.10^{-5}$) and 'DNA binding' (fold enrichment 1.64; $p = 5.56.10^{-4}$). Two mRNAs were significantly upregulated under oxidative stress: *IER2* (immediate early response protein 2) and *FOS* (AP1-transcription factor subunit), which are usually seen upregulated by environmental cues that increase intracellular levels of reactive oxygen species (Cekaite et al, 2007).

Using anti-m^{6}A antibodies, we found pervasive colocalization of the m^{6}A-modified RNAs with SGs irrespective of the type of stress, e.g. heat or oxidative stress (Fig 1A). Impairment of the 'writer' complex by combined knockdown of METTL3, METTL14 and WTAP proteins markedly decreased the colocalization of the m^{6}A signal within SGs, although overall the SGs were visible through the SG-marker protein G3BP1 (Fig 1B). It should be noted that a weak m^{6}A signal was still detectable since the 'writer' complex was silenced to 70% (Fig S2A). METTL3 is the catalytically active subunit of the complex (Roundtree et al, 2017) and its depletion alone led to a decrease of the colocalization m^{6}A signal within the SGs (Fig 1B). Generally, the 'writers' and 'erasers' resided in the nucleus under permissive growth (Fig S2B and C), where the m^{6}A modification is believed to primarily take place (Roundtree et al, 2017). In response to oxidative stress, the localization pattern of METTL14, WTAP and the 'erasers' remained unaltered (Fig S2B and C). In contrast, METTL3 partitioned between the nucleus and cytosol (Fig S2B), resembling recent observations in human cancer cells and mouse embryonic stem cells (Alarcon et al, 2015b; Lin et al, 2016). The functional cooperativity between METTL3 and METTL14 (Wang et al, 2016) requires both readers for methylation of the DRACH motifs. Thus, we cannot firmly conclude that stress-induced changes in m^{6}A modifications on mRNA take place directly in the cytosol, although they may as traces of METTL14 are also detectable in the cytosol (Fig S2B).

Since m^{6}A modulates mRNA stability (Mauer et al, 2017; Wang et al, 2014), we next determined the global effect of silenced 'writer' complex on the mRNA abundance using RNA-Seq. Overall, comparing to the total mRNAs detected under permissive growth, we did not detect substantial changes in the global mRNA levels following knockdown of the 'writer' complex (Fig 1C).

Surprisingly, when analyzing the total RNA with m^{6}A antibody, we noticed that the level of the m^{6}A signal increased upon stress and exhibited slight stress-dose dependence in both cells (Fig 1D and S2D), suggesting stress-induced increase of m^{6}A modifications. The first nucleotide in the m^{7}G cap is 2'-O-methyladenosine (A_m) which can be further methylated at N^6 position (m^6A_m) and along with the m^{6}A are targeted by the m^{6}A-antibodies (Mauer et al, 2017). Furthermore, a large fraction of non-coding RNAs (e.g. rRNA) can also be m^{6}A modified (Pan, 2013) and recognized by the m^{6}A-antibodies. Thus, a large proportion of the m^{6}A signal from the total RNA (Fig. 1D and S2D) may originate from abundant non-coding RNAs or m^6A_m modifications. To discriminate internal m^{6}A in mRNAs only, we performed global profiling of the RNA methylome (m^{6}A-Seq; (Meyer et al, 2012; Zhou et al, 2015)) in two independent biological replicates under oxidative

stress (500 µM) and permissive growth. We processed the data for each RNA biotype, which in turn allowed extracting the methylation pattern of mRNAs only. Under control growth conditions, we detected in total 8,046 m^6A peaks at consensus DRACH motifs on 4,488 unique mRNAs. Thus, from all 11,547 cellular mRNAs identified in the RNA-Seq experiment, 38.9% contained at least one m^6A peak. In response to oxidative stress (500 µM), the number of the m^6A peaks increased significantly from 8,046 to 9,142 under stress ($p = 2.8x10^{-6}$; Fig 1E and S3A). Also, the number of mRNAs with m^6A peaks increased (44.2% out of 10,791 detected total mRNAs in the RNA-Seq, $p = 2.8x10^{-6}$; Fig 1E and S3A), which supports the notion for stress-induced additional methylation of mRNAs. Thereby, these additional m^6A peaks appeared in both non-modified mRNAs but also on transcripts that were already partly methylated under control growth (Fig. S3A). m^6A modifications largely overlapped between HEK293 and U2OS cells (Fig S3B), suggesting conserved methylation pattern among different cell lines.

mRNAs associated with SGs exhibit a distinct m^6A pattern

To determine whether SG mRNA clients scored with an enriched methylation pattern, we isolated the SG mRNAs using photoactivatable ribonucleoside crosslinking and immunoprecipitation (PAR-CLIP; (Hafner et al, 2010) (Fig 2A). SGs were stabilized with 4sU-mediated crosslinking of RNAs to the RNA-binding proteins and thereafter intact SGs were isolated using established protocols (Jain et al, 2016; Khong et al, 2017). The average size of the isolated SGs (Fig S3C) was similar to the size reported previously (Kim et al, 2006). The SGs contained both mRNAs and proteins (Fig S3C and Table S1) sharing many of previously identified SG clients (Jain et al, 2016; Khong et al, 2017). To select unique mRNA clients segregated in the SGs in response to oxidative stress (500 µM), we used 2-fold enrichment over PAR-CLIP from the control, unstressed HEK-TIA1 cells and identified 6,020 unique mRNAs associated with the SGs (Fig. 2B). Using 4sU-crosslinking-based approach we identify much higher number of SG clients (e.g. 6,020 out of 10,791 total mRNAs) than described in the SG cores (Khong et al, 2017) suggesting that we captured SG clients of the whole SG, including its periphery.

54.7% of these mRNA clients were methylated (Fig 2B). Compared to the control they had significantly higher proportion of stress-induced methylation sites (Fig 2C) and higher number of methylation sites per transcript (Fig 2D). The stress-induced m^6A peaks we detected in SG mRNAs (Fig. 2C) represent 96% of all mRNAs with increased m^6A signals in response to oxidative stress (Fig 1E), suggesting that the majority of m^6A modified mRNAs reside in SGs. It should be noted that from all predicted m^6A methylation sites (e.g. DRACH motifs) only a fraction of them were m^6A modified under permissive growth or oxidative stress exposure (Fig 2D).Although we used anti-TIA1 antibodies to pull down SGs, the identified SG mRNA clients in the PAR-CLIP were enriched not only in TIA1-binding motifs (Fig S3D), implying that through the unspecific 4sU-mediated crosslinking we captured diverse mRNAs binding to different RNA-binding proteins.

We next analyzed the distribution of m^6A peaks in different transcript segments of the SG mRNA set, which were binned to equal lengths for comparison (Fig 2E). Following stress exposure m^6A peaks markedly increased in the 5'UTRs and 5' vicinity of CDSs (Fig 2E and F). In contrast, the m^6A pattern around the stop codon and 3'UTRs (Fig 2E and F) which controls mRNA stability (Meyer et al, 2012; Wang et al, 2014) was unaltered. To test the importance of the m^6A modifications in the 5' vicinity of CDS for the mRNA localization in SGs, we selected a gene, *ARL4C*, which displayed stress-induced increase in the m^6A level in this region. We introduced the first 102 nt of its CDS in-frame of *YFP* CDS and compared its localization to a variant in which the methylation sites in this region were removed. The wild-type *ARL4C-CFP* mRNA colocalized in the

hyperfluorescent SG loci (Fig. 2G). Strikingly, deletion of the methylation sites abolished the colocalization with SG and the *ARL4C-CFP* mRNA remained diffusively distributed (Fig. 2G). Collectively, these data establish a region-selective methylation of the SG following stress exposure.

Translationally-active mRNAs are methylated in the 5'UTR which does not change in response to oxidative stress

m^6A in the 5'UTR selectively regulates translation of transcripts under heat stress in a cap-independent manner (Meyer et al, 2015; Wang et al, 2015; Zhou et al, 2015) which is the prevalent mode of initiation under many stress conditions (Sonenberg & Hinnebusch, 2009). Since we also detected greater m^6A level in the 5'UTR of mRNAs following oxidative stress, we next sought to separately analyze the methylation pattern of translationally-active transcripts and those segregated in SGs. Under harsh oxidative stress (500 µM AS), translation was nearly completely inhibited (no apparent polysomal fraction; Fig S1A), thus we selected a mild stress (200 µM) at which three pools of mRNAs existed in the cytosol: actively translated ribosomes (polysomes), mRNA stalled at translation initiation (80S) and mRNAs sequestered in SGs. To identify the mRNAs in each of these states at 200 µM AS, we applied PAR-CLIP and RNA-Seq along with ribosome profiling (Ribo-Seq) (Fig 3A); in Ribo-Seq the ribosome-protected fragments (RPF) are informative on translating mRNAs (Ingolia et al, 2009). In response to mild stress (200 µM AS), we detected a significant global impairment of translation compared to the control growth (median reduction of the ribosome density of $\log_2$=2.9; Fig 3B), while transcription was unaltered (Fig S3E). At mild stress, 2,212 transcripts generated RPFs and these spanned different mRNA expression level (Fig S3F); the majority of RPFs accumulated were stalled at initiation and early elongation (Fig 3C and D), which is reminiscent of previous observation following thermal stress (Liu et al, 2013). To select genuinely translated mRNAs from the transcripts producing RPFs, we used the translation ratio (R_t) as a measure to select mRNAs with uniform RPF distribution. Following this criterion, 108 genes were selected as translated (Fig 3A and 3E and Table S2) and GO terms enriched (enrichment score 12.2) among them were 'translation' (fold enrichment 10.26; $p = 1.73.10^{-10}$), 'nonsense-mediated mRNA decay' (fold enrichment 20.37; $p = 1.43.10^{-13}$) and 'rRNA processing' (fold enrichment 11.33; $p = 2.58.10^{-10}$). These 108 translated transcripts, which compared the SG mRNAs are richer in DRACH motifs in their 5'UTRs (Fig S3G), were mostly methylated under control growth (Fig 3F) which is consistent with previous observations (Meyer et al, 2015; Zhou et al, 2015). Importantly, the m^6A level in their 5' UTR did not change following stress exposure (Fig 3F)

Many of the remaining 2,104 transcripts with RPFs displaying halted translation (e.g. $R_t > 0.5$), already these partitioned in SGs at 200 µM AS or were completely segregated in the SGs at harsh oxidative stress (500 µM AS, Fig S3H). 69.7% of these mRNAs showed stress-induced enhancement of m^6A modifications in their 5'termini at 500 µM AS. The remaining 30.3% showed no m^6A modifications, implying that their triaging into SGs is most likely driven by stress-induced stalling at initiation as described earlier (Buchan & Parker, 2009; Kedersha et al, 2013; Sonenberg & Hinnebusch, 2009). Together, these data indicate that translationally active mRNAs were highly methylated in their 5'UTRs, but stress did not induce additional m^6A modifications. In contrast, the larger fraction of mRNAs triaged to SG displayed stress-induced m^6A in their 5' UTRs and 5' vicinity of the CDS.

YTHDF3 mediates triaging of m^6A modified mRNAs to SGs under oxidative stress

Previous work has identified 'reader' proteins as evolutionary conserved cell-type-independent proteins (Edupuganti et al, 2017). These proteins selectively bind the m^{6}A moiety with their YTH domain (Dominissini et al, 2012) and regulate various aspects of RNA homeostasis. To gain mechanistic understanding on the participation of 'reader' proteins in mRNA recruitment to SGs through selective recognition of the m^{6}A sites, we analyzed the distribution of three YTH-domain-containing proteins in USO2-G3BP1 cells exposed to 500 µM AS. YTHDF3 colocalized exclusively with the SGs, YTHDF1 exhibited only marginal colocalization with SGs, while YTHDF2 retained its cytoplasmic localization (Fig 4A). At ambient growth conditions, YTHDF1 and YTHDF2 partitioned between cytosol and nucleus, while YTHDF3 resided in the cytosol (Fig S4A) which is in agreement with previous observations (Li et al, 2017; Meyer et al, 2015; Zhou et al, 2015). Importantly, a knockdown of the 'writer' complex completely abolished the YTHDF3 localization in SGs but had no noticeable effect on YTHDF1 partitioning into SGs (Fig 4A). Also, siRNA-mediated silencing of *YTHDF3* (Fig 4B and S4B) abrogated the colocalization of the m^{6}A signal with the SGs, suggesting new role of YTHDF3 'reader' in recruiting m^{6}A-modified mRNAs into SGs. Similarly to the 'writer' complex silencing (Fig1B), the knock-down of *YTHDF3* did not change the overall formation of SGs as detected through the SG-scaffold protein G3BP1 (Fig 4B). Importantly, knockdown of the 'writer' complex or YTHDF3 decreased markedly the amount of m^{6}A-modified mRNA in SGs, while the amount of non-methylated mRNAs in SGs, detected through the polyA-tag, was influenced to much lower extent (Fig. 4C); the latter correlates with the observation that 45.3% of all transcripts found in the SGs were not methylated (Fig. 2B).

To stratify the specificity of YTHDF3 towards SG substrates, we integrated our m^{6}A-Seq and PAR-CLIP data on SGs with recently published YTHDF3 PAR-CLIP data (Shi et al, 2017). A substantial amount of the genes identified as YTHDF3 clients overlapped with the SG clients (Fig 4D), whereas the overlap with the YTHDF1 and YTHDF2 is much smaller (Fig S4C and D). Together, our results reveal YTHDF3 as a mediator in triaging mRNAs methylated in their 5' termini to SGs under oxidative stress.

Discussion

SGs are crucial for facilitating stress response and reprogramming gene expression to maximize cell survival under stress. Our results revealed two modes of triaging mRNAs into SGs following oxidative stress. For the larger fraction of mRNAs (appr 55 %) stress-induced m^{6}A modifications in the 5' vicinity of the transcripts serve as a specific mechanism for triaging them into SGs (Fig 5). The significance of m^{6}A residues for triaging mRNAs to SGs is further supported by our finding that deletion of DRACH motifs in the 5' termini of the CDS abrogates the localization of the transcript in SGs (Fig 2G). Another fraction of mRNAs (appr. 45%), which are not methylated, most likely associate with the SGs triggered by the oxidative stress-induced stalling at initiation (Fig 5) as suggested earlier (Buchan & Parker, 2009; Kedersha et al, 2013; Sonenberg & Hinnebusch, 2009). However, it is possible that stalled ribosomes at initiation and/or early elongation (Fig. 3C) would sterically hinder the methylation in these regions. Thus, we may be underestimating the fraction of methylated mRNAs and the stress-induced methylation in the 5' termini might be more prevalent.

In contrast, to the wide belief that m^{6}A modification is static on mRNAs, we found that the 5'UTR and 5' vicinity of CDSs methylation is dynamic and induced by oxidative stress. This stress-inducible methylation is recognized by YTHDF3 reader which relocates those transcripts to SGs

(Fig. 5). Supportive for the notion that the process is directly mediated by YTHDF3 is our observation that YTHDF3 partitioning in SGs is altered following silencing of methylation, while the localization of YTHDF1 and YTHDF2 is unaltered. SGs are enriched with proteins containing IDRs or QN-rich prion-like domains with high intrinsic propensity to self-aggregate through hetero- and homotypic interaction (Gilks et al, 2004; Jain et al, 2016; Lin et al, 2015; Toretsky & Wright, 2014). This idea is supported by *in vitro* observations wherein high concentrations of proteins with IDRs are sufficient to spontaneously form liquid-like droplets (Kato et al, 2012; Lin et al, 2015; Molliex et al, 2015). Structural predictions of the YTH-domain readers with DisEMBL revealed QN-rich IDRs in all three proteins, e.g. 282-303 aa, 249-299 aa and 315-351 aa for YTHDF1, YTHDF2 and YTHDF3, respectively. Hence, it is conceivable that the YTH-domain 'reader' proteins, all of which found in the SGs (Table S1 and (Jain et al, 2016)), are sequestered in the SGs through unspecific IDR-driven interactions with other SG proteins. Although we cannot exclude a cooperativity among three YTH-domain readers, clearly only YTHDF3 binds to the stress-induced m^6A on mRNAs and most likely through protein-protein interactions with its IDR relocates them to SG (Fig 5).

Earlier studies propose that SGs are nucleated by translationally-stalled RNAs with assembled initiation factors which serve as scaffolds for RNA-binding proteins (Decker & Parker, 2012; Kedersha et al, 2013). Hence, the primary nucleation of SGs might occur in m^6A-independent manner involving the fraction of mRNAs we detect as non-methylated following stress exposure (Fig. 5). Recent study shows that the core SG protein, G3BP1, which nucleates SGs (Kedersha et al, 2016), is repelled by m^6A (Edupuganti et al, 2017) and thus, might be recruited exclusively to mRNAs lacking m^6A modification. Consistent with this model is our observation that silencing of the 'writer' complex alters only the association of m^6A-modified mRNAs and YTHDF3 with SGs, but not the SG formation in general. Conceivably, the SG nucleation and core formation might occur in m^6A-independent manner involving primarily non-translating mRNAs stalled at initiation, while the methylation-driven association of mRNAs might take place in the more dynamic SGs periphery (Fig. 5).

Our studies show that mRNAs genuinely translated under oxidative stress are enriched in m^6A signals in their 5' UTRs. Unlike the SG clients which are dynamically methylated under stress, the translated pool exhibits high basal methylation (e.g. under permissive growth) which remains unchanged under stress. This raises the intriguing question as to how YTHDF3 reader discriminates those from SG clients. Under permissive growth, translation of selected transcripts is enhanced by YTHDF1 which binds to select transcripts at m^6A in their 3'UTRs (Wang et al, 2015). YTHDF1 binds simultaneously then to ribosomal proteins of already assembled initiating ribosome to influence the cap-dependent translation (Li et al, 2017). Although YTHDF3 itself can also associate with ribosomal proteins and m^6A modified 3'UTRs (Li et al, 2017; Shi et al, 2017), it does not compete but rather facilitates YTHDF1 biding (Li et al, 2017). Our data show that deletion of DRACH motifs in the 5' termini of the CDS alone is sufficient to abrogate the YTHDF3-mediated localization of the transcript in SGs (Fig 2G) that supports the notion that the 5' termini of the CDS and not the 5' UTRs are likely the primary binding site of YTHDF3 reader. The YTHDF3 binding to 5' termini in the CDS may then sterically hinder initiated ribosomes to commence elongation. Or, depletion of YTHDF3 from the YTHDF1-YTHDF3-ribosome complex may weaken the YTHDF1 interactions and cause dissociation of the initiation complex. Although the downstream effect is unknown, it is clear, that YTHDF3 relocate m^6A-modified mRNA in SGs as siRNA-mediated decrease in its concentration abrogates this process. This unexpected feature of YTHDF3 protein in triaging mRNAs to SGs offers a mechanism for dynamic control of the localization of mRNAs during stress.

Materials and Methods

Cell culture and siRNA-mediated gene silencing

U2OS cells, stably expressing GFP tagged SG marker G3BP1 or P-body marker DCP1 (Ohn et al, 2008) or HEK293 expressing N-terminally FLAG-tagged TIA1 under doxycycline-dependent promoter (Damgaard & Lykke-Andersen, 2011) were maintained in Dulbecco's modified Eagle's medium (DMEM), supplemented with 10% FBS, penicillin/streptamycin 250 U, glutamine 2 mM). For simplicity, cells are called U2OS-G3BP1, U2OS-DCP1 and HEK-TIA1. All cell lines were grown at 37°C in a humidified atmosphere with 5% CO_2. Oxidative stress was elicited by adding sodium arsenite (AS) for 30 min at 37°C at 70-80% confluency. Thermal stress was exerted by incubating the cells at 42 °C for 2 h. First 102 nt of the CDS of *ARL4C* gene were fused in-frame in lieu of the Met codon of CFP. In parallel, three DRACH motifs in the 102-nt *ARL4C* region were synonymously replaced so that the amino acid sequence remained unaltered. Both constructs were cloned into pcDNA vector and used for transient transfections.
For siRNA-mediated gene silencing, U2OS-G3BP1 cells were grown to 50% confluency in 6-well plates, transfected with 10 mM siRNA unless otherwise stated dissolved in 4 µL jet prime transfection reagent and 200 µM transfection buffer (PolyPlus) and analyzed 48h after transfection. siRNA sequences that target *METTL3*, *METTL14* and *WTAP* were as follows: *METTL3*, 5'-CUGCAAGUAUGUUCACUAUGATT-3', *METTL14*, 5'-AAGGAUGAGUUAAUAGCUAAATT-3'; *WTAP,* 5'-GGGCAAGUACACAGAUCUUAATT-3'. Two deoxynucelotides (TT) were added for in-cell stabilization of the oligonucleotides.

Fluorescence *in situ* hybridization (FISH)

Two 25-mer DNA oligonucleotides with sequence complementary to the *ADAMTS*1, *ADAMTS3*, *ADAMTS8* and *ADAMTS15* sequences:
5'-AGATAGCGTCCTTCTAGATTTGTGCTGACTGGAGTCACCAGCTCATACTC-3' and
5'- GAGTATGAGCTGGTGACTCCAGTCAGCACAAATCTAGAAGGACGCTATCT-3' were annealed in 1x DNA polymerase reaction buffer (Thermo, Germany) by heating briefly to 95°C and slowly cooled down to room temperature. To 2 µg of annealed oligonucleotides 1 mM of three unlabeled dNTPs (dGTP, dATP and dCTP), 0.2 mM Cy5-labeled dTNP, 0.2 U/µL of DNase I, DNA Polymerase I (5-15 U) were added in nuclease-free water (40 µL total volume). Samples were incubated for 15-60 min and purified by standard ethanol precipitation approach.
U2OS-G3BP1 cells grown to 70% confluency were fixed with 10% PFA for 10 min at room temperature and permeabilized overnight at 4°C with 70% ethanol. Cells were rehydrated with rehydration buffer (2x SSC; 300 mM NaCl, 30 mM sodium citrate, pH 7.0, containing 50% formamide) and incubated overnight at 37°C with 30 ng FISH probe dissolved in hybridization buffer (2x SSC containing 10% dextran sulfate, 2 mM vanadyl-ribonucleoside complex, 0.02% RNAse-free BSA, 40 µg *E.coli* total tRNA, 50% formamide). Cells were washed twice in rehydration buffer for 30 min and imaged on Olympus IX81 confocal microscope.

Polysome fractionation

Cells at 70-80% confluency were pelleted at 850xg and respuspended in polysome lysis buffer (10 mM Tris-HCl (pH 7.4), 5 mM $MgCl_2$, 100 mM KCl, 1% Triton X-100, supplemented with 2 mM DTT and 100 µg/ml cicloheximide). Lysis was performed by sharing 8-9 times through 21G needle. 300 µL of lysate was loaded onto 5-ml sucrose gradient (50% to 15% sucrose in, 50 mM HEPES-KOH,

pH 7.4, 50 mM $MgCl_2$, 100 mM KCl, 2 mM cycloheximide, 2 mM DTT) and separated by ultracentrifugation at 148,900xg (Beckman, Ti55 rotor) for 1.5 hours at 4°.

PAR-CLIP of SGs

PAR-CLIP was performed following the published protocol (Spitzer et al, 2014) using 4-thiouridine(4sU)-mediated mRNA crosslinking to RNA-binding proteins. Briefly, HEK-TIA1 cells (70% confluent) were supplemented with 4sU to a final concentration of 100 µM and incubated for 16 h prior to exposure to stress with 200 or 500 µM AS at 37°C for 30 min. Cells were crosslinked with 1500 µJ/cm² at 365 nm, washed once with ice-cold PBS and lysed in lysis buffer (20 mM Tris-HCl pH 7.4, 15 mM NaCl, 1% NP-40, 0.1% triton-X, protease inhibitor) by pipetting up and down 8x using a 26G syringe. Supernatant was cleared at 16,000xg for 10 min and subjected to immunoprecipitation with anti-FLAG antibody-coated magnetic beads. In a parallel procedure, SGs were isolated without 4sU incorporation using crosslinking at 254 nm (1500 µJ/cm^2).
100 µL protein G coated Dynabeads or Macs protein G micro beads were washed twice with lysis buffer and incubated with 2 µg of anti-FLAG antibody for 1 h at room temperature. Antibody solution was removed and beads were washed 3x with 900 µl lysis buffer. After incubation with the cell lysate from HEK-TIA1 cells for 2 hours at 4°C, beads were carefully washed twice with washing buffer (20 mM Tris-HCl pH 7.4, 150 mM NaCl, 1% NP-40, 0.1% triton-X, protease inhibitor) and directly subjected to RNA extraction for RNA sequencing.

RNA isolation, RNA-Seq and Ribo-Seq

RNA was extracted by adding 0.1 volume of 10% SDS, one volume of acidic phenol-chlorophorm (5:1, pH 4.5) preheated to 65°C and incubated at 65°C for 5 min. The reaction was cooled on ice for 5 min. Phases were separated by centrifugation at 21,000xg for 5 min. Equal volume of acid phenol-chloroform was added to the aqueous phase, separated by centrifugation and supplemented with an equal volume of chloroform:isoamyl alcohol (24:1). Upon separation, the aqueous phase was supplemented with 0.1 vol 3M NaOAc (pH 5.5) and an equal volume of isopropanol. Samples were precipitated for 3 h at -20°C. RNA was pelleted at 21,000xg at 4°C, and the dried pellets resuspended in DEPC-H_2O. ERCC RNA Spike-Ins were added upon rRNA depletion using Ribo-Zero Magnetic Gold Kit and used to set the detection threshold in each sequencing set. The rRNA-depleted samples were fragmented in alkaline fragmentation buffer (0.5 vol 0.5 M EDTA, 15 vol 100 mM Na_2CO_3, 110 vol 100 mM $NaHCO_3$), dephosphorylated and fragments ranging from 20-35 nt were size-selected on 15% polyacrylamide gel containing 8M urea. The adapters were ligated directly to the 5'- and 3'-ends as previously described (Guo et al, 2010), converted into cDNA libraries and sequenced on a HiSeq2000 (Illumina) machine.
Approximately five million HEK 293-TIA1 cells, unstressed or stressed with 200 µM AS for 30 min, each in two independent biological replicates, were used to isolate mRNA-bound ribosome complexes, followed by extraction of RNase I digested ribosome-protected fragments (RPFs) as previously described (Guo et al, 2010; Kirchner et al, 2017). Cells were collected by flash-freezing without preincubation with antibiotics and cDNA libraries from RPFs were prepared with direct ligation of the adapters (Guo et al, 2010; Kirchner et al, 2017) and sequenced on a HiSeq2000 (Illumina) machine.

m^6A-Sequencing (m^6A-Seq)

Total RNA from approximately 45 million HEK 293-TIA1 cells, unstressed or stressed with 500 µM AS for 30 min, was first isolated using Trizol reagent followed by fragmentation using freshly prepared RNA fragmentation buffer (10 mM Tris-HCl, pH 7.0, 10 mM $ZnCl_2$). 5 µg fragmented

RNA was saved for RNA-Seq as input control. For m^{6}A-Seq, 400 µg fragmented RNA was incubated with 10 µg anti-m^{6}A antibody (Millipore, ABE572) and 2.5 µg anti-m^{6}A antibody (Synaptic Systems, #202203) in 1×IP buffer (10 mM Tris-HCl, pH 7.4, 150 mM NaCl, and 0.1% Igepal CA-630) for 2 h at 4°C. The m^{6}A-IP mixture was then incubated with Protein A/G beads for additional 2 h at 4°C on a rotating wheel. After washing 3x with IP buffer, bound RNA was eluted using 100 µl elution buffer (6.7 mM N^6-methyladenosine 5'-monophosphate sodium salt in 1× IP buffer), followed by ethanol precipitation. Precipitated RNA was used for cDNA library construction and high-throughput sequencing described below.

Preprocessing of the sequencing reads

Sequencing reads were trimmed using *fastx-toolkit* (quality threshold: 20), adapters were cut using *cutadapt* (minimal overlap: 1 nt), and processed reads were mapped to the human genome (GRCh37) using Bowtie either uniquely or allowing multimapping with a maximum of two mismatches (parameter settings: -l 16 -n 1 -e 50 -m 1 or 10 --strata --best y). Uniquely mapped RPF reads (Ribo-Seq), or fragmented RNA reads (RNA-Seq), were normalized as reads per million mapped reads (RPM) or reads per kilobase per million mapped reads (RPKM). All sequencing reactions were performed in biological replicates. Based on the high correlation between the replicates (R^2 > 0.9 for all data sets, Person coefficient), reads from biological replicates were merged into metagene sets (Ingolia et al, 2009).

m^{6}A-Seq and input RNA-Seq reads (20nt – 40nt) were aligned to NCBI RefSeq mRNA sequences and UCSC genome sequences (hg19 for human) using Tophat (--bowtie1 --no-novel-juncs -G) as described previously (Trapnell et al, 2009).

Dataset processing

Under control growth conditions the majority of the transcribed mRNAs were also translated in HEK-TIA1 cells (Fig S4F). The ribosome density (RD) for each transcript (previously defined as "translation efficiency" or TE (Ingolia et al, 2009)), was computed as follows:

$$RD = \frac{\text{RPF [RPM]}}{\text{mRNA [RPM]}} \quad (1)$$

RD values of all protein-coding genes were normalized to the RD of mitochondrial genes as described (Iwasaki et al, 2016). Mitochondrial genes were used for normalization as their expression under stress remained unchanged.

Cumulative profiles of the read density for RPFs and mRNA have been computed as described (Gerashchenko et al, 2012). High ribosome occupancy at the start of the coding sequence (CDS) following exposure to oxidative stress indicated that not all RPFs reported translation (Fig 3C). To distinguish between genuinely translated transcripts and those whose translation was inhibited by stress, we set the following ratio R_t:

$$R_t = \frac{total\ RPF\ reads\ of\ initial\ stalled\ peak\ (first\ 100nt)[RPKM]}{total\ RPF\ reads\ over\ the\ full\ gene\ [RPKM]} \quad (2)$$

At 200 µM AS 108 mRNAs exhibited $R_t \leq 0.5$ and were considered as actively translated. Whereas for 2,104 genes we detected RPFs largely stalled at initiation with $R_t > 0.5$ and designated them as triaged for SG.

In the PAR-CLIP experiments, SG clients in cells stressed with 200 or 500 µM AS were selected using a threshold of $\log_2$=2 over control growth. The variability between biological replicates in the

PAR-CLIP experiments (Pearson correlation coefficient) from cells exposed to 200 or 500 µM AS was R^2 = 0.695 and 0.735, respectively. Furthermore, the correlation between the selected SG clients at both stress conditions was very high (Fig S3G). The data set at 200 µM AS comprises PAR-CLIP detected and triaged in the Ribo-Seq (Fig 3D). The majority of the transcripts identified in the Ribo-Seq with halted translation and designated as triaged for SG were also found among the SG clients at harsh stress (500 µM AS). Thus, all selected mRNAs (either in the PAR-CLIP data sets or designated as triaged in the Ribo-Seq) were merged together into a metagene set of SG clients containing in total 6,020 transcripts. These mRNAs found in SGs span a large expression range (Fig S3F). Statistical analysis was mainly done in R and SigmaPlot (Systat Software).

Motif analysis

De novo search for DRACH motifs was performed using FIMO and the threshold was at $p<0.001$. The corresponding transcript groups were prepared with Ensembl Biomart. For comparing the number of DRACH motifs in each transcript region, 5'UTRs, CDSs and 3'UTRs were divided into equal bins for comparable length and the amount of motifs in each segment was averaged over the whole gene set in the selected group. General motif search among the SG clients was performed using MEME suite. Gene function analysis (GO enrichment) was performed with the DAVID tool.

Identification of the m^{6}A sites

All full-length mapped reads were used to generate m^{6}A-Seq coverage profile for individual genes. To compare metagene m^{6}A profiles between control and stress (500 µM AS) samples, the raw coverage values were first internally normalized by the mean coverage of each individual gene (for genes with multiple mRNA isoforms, the longest isoform was selected). The genes with maximal coverage value less than 15 were excluded from further consideration. The normalized m^{6}A-Seq profiles of individual gene were next subtracted by corresponding RNA-Seq profile to generate an adjusted m^{6}A-Seq profile. The metagene profile used for between-sample comparison (control vs. stress) was finally derived by averaging all adjusted profiles of individual genes.
The identified m^{6}A peaks in the m^{6}A-Seq were assigned to the predicted DRACH motifs. Peaks occurring in regions that cover at least one predicted DRACH motif were selected for further analysis. If more than one DRACH motif was found within m^{6}A peak, all of them have been considered as methylated. Metagene profiles of the distribution of the m^{6}A sites along different transcript segments (Fig 2F) were performed by determining the ratio between m^{6}A-modified DRACH motifs detected in m^{6}A-Seq and total number of predicted DRACH motifs in each transcript segment. To compare the m^{6}A peaks in HEK-TIA1 to those of U2OS-cells from a previously published m^{6}A-Seq data set (Xiang et al, 2017), the m^{6}A-modified DRACH motifs identified in HEK-TIA1 were compared to those in U2OS (Fig S3B).

Dataset availability

Deep sequencing data from RNA-Seq, Ribo-Seq, PAR-CLIP and m^{6}A-Seq were deposited in the BioSample data base (https://www.ncbi.nim.nih.gov/biosample/) under accession number SRP121376.

Acknowledgements

We are grateful to Dr. Hartmut Schlüter and Parnian Kiani from the mass spectrometry core facility UKE, Hamburg, for the help with mass spectrometry analysis. We thank Lindsey Bultema for the

TEM images. This work was supported by grants to Z.I. from the Deutsche Forschungsgemeinschaft (DFG; IG73/14-1 and IG73/14-2).

References

Alarcon CR, Goodarzi H, Lee H, Liu X, Tavazoie S, Tavazoie SF (2015a) HNRNPA2B1 Is a Mediator of m(6)A-Dependent Nuclear RNA Processing Events. *Cell* 162**:** 1299-1308

Alarcon CR, Lee H, Goodarzi H, Halberg N, Tavazoie SF (2015b) N6-methyladenosine marks primary microRNAs for processing. *Nature* 519**:** 482-485

Andreev DE, O'Connor PB, Fahey C, Kenny EM, Terenin IM, Dmitriev SE, Cormican P, Morris DW, Shatsky IN, Baranov PV (2015) Translation of 5' leaders is pervasive in genes resistant to eIF2 repression. *Elife* 4**:** e03971

Buchan JR, Parker R (2009) Eukaryotic stress granules: the ins and outs of translation. *Mol Cell* 36**:** 932-941

Cekaite L, Peng Q, Reiner A, Shahzidi S, Tveito S, Furre IE, Hovig E (2007) Mapping of oxidative stress responses of human tumor cells following photodynamic therapy using hexaminolevulinate. *BMC Genomics* 8**:** 273

Coots RA, Liu XM, Mao Y, Dong L, Zhou J, Wan J, Zhang X, Qian SB (2017) m(6)A Facilitates eIF4F-Independent mRNA Translation. *Mol Cell* 68:504-514.

Damgaard CK, Lykke-Andersen J (2011) Translational coregulation of 5'TOP mRNAs by TIA-1 and TIAR. *Genes Dev* 25**:** 2057-2068

Decker CJ, Parker R (2012) P-bodies and stress granules: possible roles in the control of translation and mRNA degradation. *CSH Perspect Biol* 4**:** a012286

Dominissini D, Moshitch-Moshkovitz S, Schwartz S, Salmon-Divon M, Ungar L, Osenberg S, Cesarkas K, Jacob-Hirsch J, Amariglio N, Kupiec M et al (2012) Topology of the human and mouse m6A RNA methylomes revealed by m6A-seq. *Nature* 485**:** 201-206

Edupuganti RR, Geiger S, Lindeboom RGH, Shi H, Hsu PJ, Lu Z, Wang SY, Baltissen MPA, Jansen P, Rossa M et al (2017) N6-methyladenosine (m6A) recruits and repels proteins to regulate mRNA homeostasis. *Nat Struct Mol Biol* 24:870-878

Gerashchenko MV, Lobanov AV, Gladyshev VN (2012) Genome-wide ribosome profiling reveals complex translational regulation in response to oxidative stress. *Proc Natl Acad Sci* 109**:** 17394-17399

Gilks N, Kedersha N, Ayodele M, Shen L, Stoecklin G, Dember LM, Anderson P (2004) Stress granule assembly is mediated by prion-like aggregation of TIA-1. *Molecular biology of the cell* 15**:** 5383-5398

Guo H, Ingolia NT, Weissman JS, Bartel DP (2010) Mammalian microRNAs predominantly act to decrease target mRNA levels. *Nature* 466**:** 835-840

Hafner M, Landthaler M, Burger L, Khorshid M, Hausser J, Berninger P, Rothballer A, Ascano M, Jr., Jungkamp AC, Munschauer M et al (2010) Transcriptome-wide identification of RNA-binding protein and microRNA target sites by PAR-CLIP. *Cell* 141**:** 129-141

Ingolia NT, Ghaemmaghami S, Newman JR, Weissman JS (2009) Genome-wide analysis in vivo of translation with nucleotide resolution using ribosome profiling. *Science* 324**:** 218-223

Iwasaki S, Floor SN, Ingolia NT (2016) Rocaglates convert DEAD-box protein eIF4A into a sequence-selective translational repressor. *Nature* 534**:** 558-561

Jain S, Wheeler JR, Walters RW, Agrawal A, Barsic A, Parker R (2016) ATPase-Modulated Stress Granules Contain a Diverse Proteome and Substructure. *Cell* 164**:** 487-498

Kato M, Han TW, Xie S, Shi K, Du X, Wu LC, Mirzaei H, Goldsmith EJ, Longgood J, Pei J et al (2012) Cell-free formation of RNA granules: low complexity sequence domains form dynamic fibers within hydrogels. *Cell* 149**:** 753-767

Kedersha N, Ivanov P, Anderson P (2013) Stress granules and cell signaling: more than just a passing phase? *Trends Biochem Sci* 38**:** 494-506

Kedersha N, Panas MD, Achorn CA, Lyons S, Tisdale S, Hickman T, Thomas M, Lieberman J, McInerney GM, Ivanov P et al (2016) G3BP-Caprin1-USP10 complexes mediate stress granule condensation and associate with 40S subunits. *J Cell Biol* 212**:** 845-860

Kedersha N, Stoecklin G, Ayodele M, Yacono P, Lykke-Andersen J, Fritzler MJ, Scheuner D, Kaufman RJ, Golan DE, Anderson P (2005) Stress granules and processing bodies are dynamically linked sites of mRNP remodeling. *J Cell Biol* 169**:** 871-884

Khong A, Matheny T, Jain S, Mitchell SF, Wheeler JR, Parker R (2017) The Stress Granule Transcriptome Reveals Principles of mRNA Accumulation in Stress Granules. *Mol Cell* 68**:** 808-820 e805

Kim SH, Dong WK, Weiler IJ, Greenough WT (2006) Fragile X mental retardation protein shifts between polyribosomes and stress granules after neuronal injury by arsenite stress or in vivo hippocampal electrode insertion. *J Neurosci* 26**:** 2413-2418

Kirchner S, Cai Z, Rauscher R, Kastelic N, Anding M, Czech A, Kleizen B, Ostedgaard LS, Braakman I, Sheppard DN et al (2017) Alteration of protein function by a silent polymorphism linked to tRNA abundance. *PLoS Biol* 15**:** e2000779

Li A, Chen YS, Ping XL, Yang X, Xiao W, Yang Y, Sun HY, Zhu Q, Baidya P, Wang X et al (2017) Cytoplasmic m(6)A reader YTHDF3 promotes mRNA translation. *Cell Res* 27**:** 444-447

Lin S, Choe J, Du P, Triboulet R, Gregory RI (2016) The m(6)A Methyltransferase METTL3 Promotes Translation in Human Cancer Cells. *Mol Cell* 62**:** 335-345

Lin Y, Protter DS, Rosen MK, Parker R (2015) Formation and Maturation of Phase-Separated Liquid Droplets by RNA-Binding Proteins. *Mol Cell* 60**:** 208-219

Liu B, Han Y, Qian SB (2013) Cotranslational response to proteotoxic stress by elongation pausing of ribosomes. *Mol Cell* 49**:** 453-463

Liu N, Dai Q, Zheng G, He C, Parisien M, Pan T (2015) N(6)-methyladenosine-dependent RNA structural switches regulate RNA-protein interactions. *Nature* 518**:** 560-564

Mauer J, Luo X, Blanjoie A, Jiao X, Grozhik AV, Patil DP, Linder B, Pickering BF, Vasseur JJ, Chen Q et al (2017) Reversible methylation of m6Am in the 5' cap controls mRNA stability. *Nature* 541**:** 371-375

Meyer KD, Jaffrey SR (2017) Rethinking m6A Readers, Writers, and Erasers. *Ann Rev Cell Develop Biol* 33: 319-342.

Meyer KD, Patil DP, Zhou J, Zinoviev A, Skabkin MA, Elemento O, Pestova TV, Qian SB, Jaffrey SR (2015) 5' UTR m(6)A Promotes Cap-Independent Translation. *Cell* 163**:** 999-1010

Meyer KD, Saletore Y, Zumbo P, Elemento O, Mason CE, Jaffrey SR (2012) Comprehensive analysis of mRNA methylation reveals enrichment in 3' UTRs and near stop codons. *Cell* 149**:** 1635-1646

Molliex A, Temirov J, Lee J, Coughlin M, Kanagaraj AP, Kim HJ, Mittag T, Taylor JP (2015) Phase separation by low complexity domains promotes stress granule assembly and drives pathological fibrillization. *Cell* 163**:** 123-133

Munteanu A, Mukherjee N, Ohler U (2018) SSMART: Sequence-structure motif identification for RNA-binding proteins. *bioRXiv*

Ohn T, Kedersha N, Hickman T, Tisdale S, Anderson P (2008) A functional RNAi screen links O-GlcNAc modification of ribosomal proteins to stress granule and processing body assembly. *Nat Cell Biol* 10**:** 1224-1231

Pan T (2013) N6-methyl-adenosine modification in messenger and long non-coding RNA. *Trends Biochem Sci* 38**:** 204-209

Panas MD, Ivanov P, Anderson P (2016) Mechanistic insights into mammalian stress granule dynamics. *J cell Biol* 215**:** 313-323

Protter DS, Parker R (2016) Principles and Properties of Stress Granules. *Trends Cell Biol* 26**:** 668-679

Roundtree IA, Evans ME, Pan T, He C (2017) Dynamic RNA Modifications in Gene Expression Regulation. *Cell* 169**:** 1187-1200

Shi H, Wang X, Lu Z, Zhao BS, Ma H, Hsu PJ, Liu C, He C (2017) YTHDF3 facilitates translation and decay of N6-methyladenosine-modified RNA. *Cell Res* 27**:** 315-328

Sonenberg N, Hinnebusch AG (2009) Regulation of translation initiation in eukaryotes: mechanisms and biological targets. *Cell* 136**:** 731-745

Spitzer J, Hafner M, Landthaler M, Ascano M, Farazi T, Wardle G, Nusbaum J, Khorshid M, Burger L, Zavolan M et al (2014) PAR-CLIP (Photoactivatable Ribonucleoside-Enhanced Crosslinking and Immunoprecipitation): a step-by-step protocol to the transcriptome-wide identification of binding sites of RNA-binding proteins. *Meth Enzymol* 539**:** 113-161

Toretsky JA, Wright PE (2014) Assemblages: functional units formed by cellular phase separation. *J Cell Biol* 206**:** 579-588

Trapnell C, Pachter L, Salzberg SL (2009) TopHat: discovering splice junctions with RNA-Seq. *Bioinformatics* 25**:** 1105-1111

Wang P, Doxtader KA, Nam Y (2016) Structural Basis for Cooperative Function of Mettl3 and Mettl14 Methyltransferases. *Mol Cell* 63**:** 306-317

Wang X, Lu Z, Gomez A, Hon GC, Yue Y, Han D, Fu Y, Parisien M, Dai Q, Jia G et al (2014) N6-methyladenosine-dependent regulation of messenger RNA stability. *Nature* 505**:** 117-120

Wang X, Zhao BS, Roundtree IA, Lu Z, Han D, Ma H, Weng X, Chen K, Shi H, He C (2015) N(6)-methyladenosine Modulates Messenger RNA Translation Efficiency. *Cell* 161**:** 1388-1399

Xiang Y, Laurent B, Hsu CH, Nachtergaele S, Lu Z, Sheng W, Xu C, Chen H, Ouyang J, Wang S et al (2017) RNA m6A methylation regulates the ultraviolet-induced DNA damage response. *Nature* 543**:** 573-576

Zhou J, Wan J, Gao X, Zhang X, Jaffrey SR, Qian SB (2015) Dynamic m(6)A mRNA methylation directs translational control of heat shock response. *Nature* 526**:** 591-594

Figure legends:

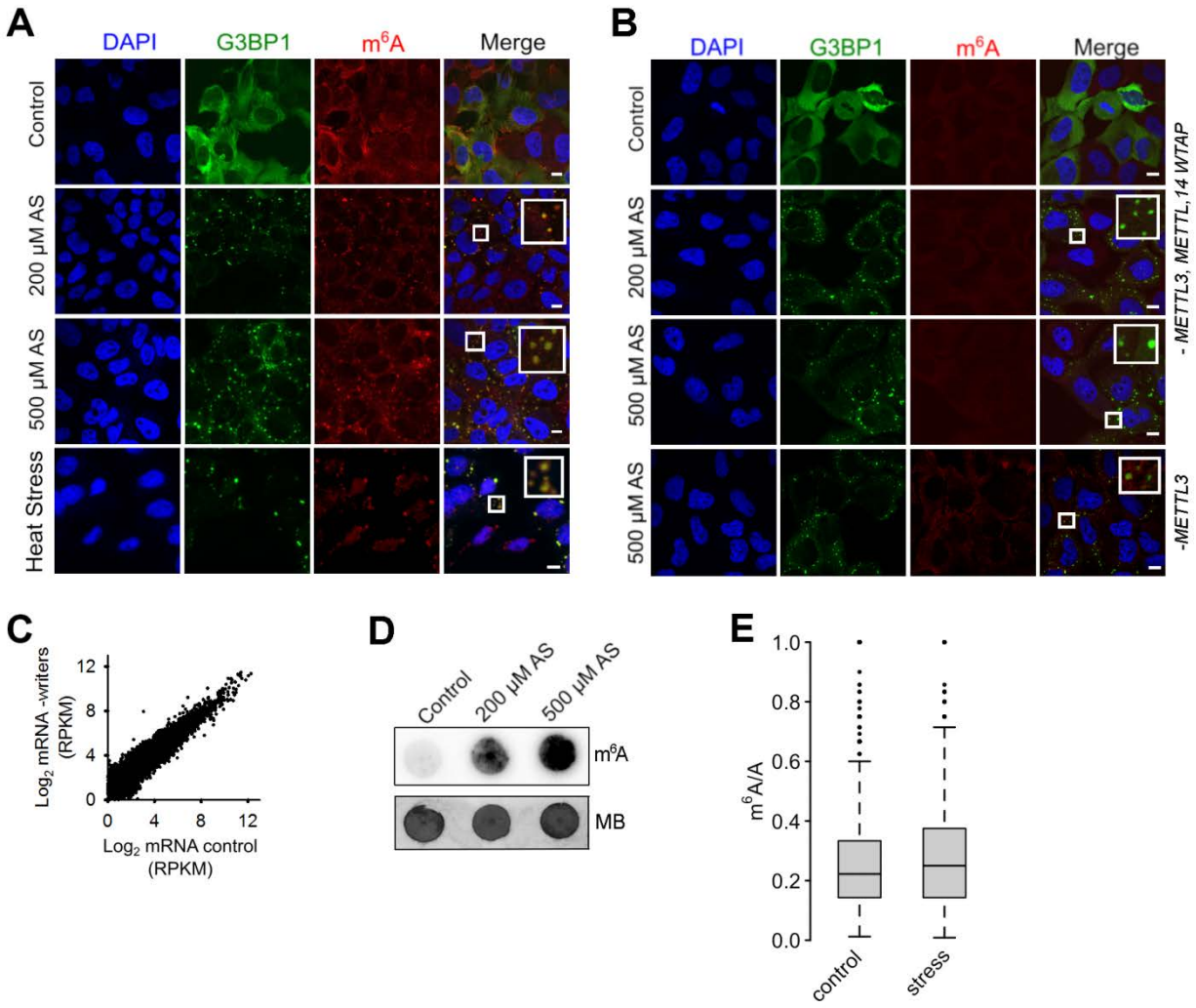

Figure 1 – m^{6}A signal increases in response to oxidative stress and accumulates in SGs
(A) U2OS-G3BP1 cells grown under permissive conditions (control) or exposed to mild (200 µM AS) or harsh (500 µM AS) oxidative stress for 30 min, or to heat for 2 h at 42°C and immunostained with anti-m^{6}A antibody. SG (hyperfluorescent loci) were visualized through G3BP1–GFP (green), nuclei were counterstained with DAPI (blue). Scale bar, 10 µm. **(B)** Combined siRNA knockdown of the 'writer' complex (*METTL3*, *METTL14* and *WTAP*) or *METTL3* alone (lowest row) in U2OS-G3BP1 cells. *METTL3*, *METTL14* or *WTAP* were silenced to maximally 70% resulting in some residual m^{6}A immunostaining (Fig S2A). Scale bar, 10 µM. **(C)** Comparison of the expression of total mRNA in control growth and following siRNA-mediated knockdown of the 'writer' complex (-writers) in HEK-TIA1 cells determined by RNA-Seq. R^2= 0.928, Pearson correlation coefficient. **(D)** Total RNA isolated from the same amount of U2OS-G3BP1 cells grown at permissive (control) conditions or exposed to various AS concentrations and detected with m^{6}A antibody or methylene blue (MB). **(E)** Box-plot of m^{6}A sites (from the m^{6}A-Seq) detected across all mRNAs of untreated cells (control) or exposed to stress (500 µM AS) and presented as a ratio of the total m^{6}A sites (e.g. predicted DRACH motifs designated as A in the ratio m^{6}A/A). p = 2.8x10^{-6} control vs. stress, Mann-Whitney test.

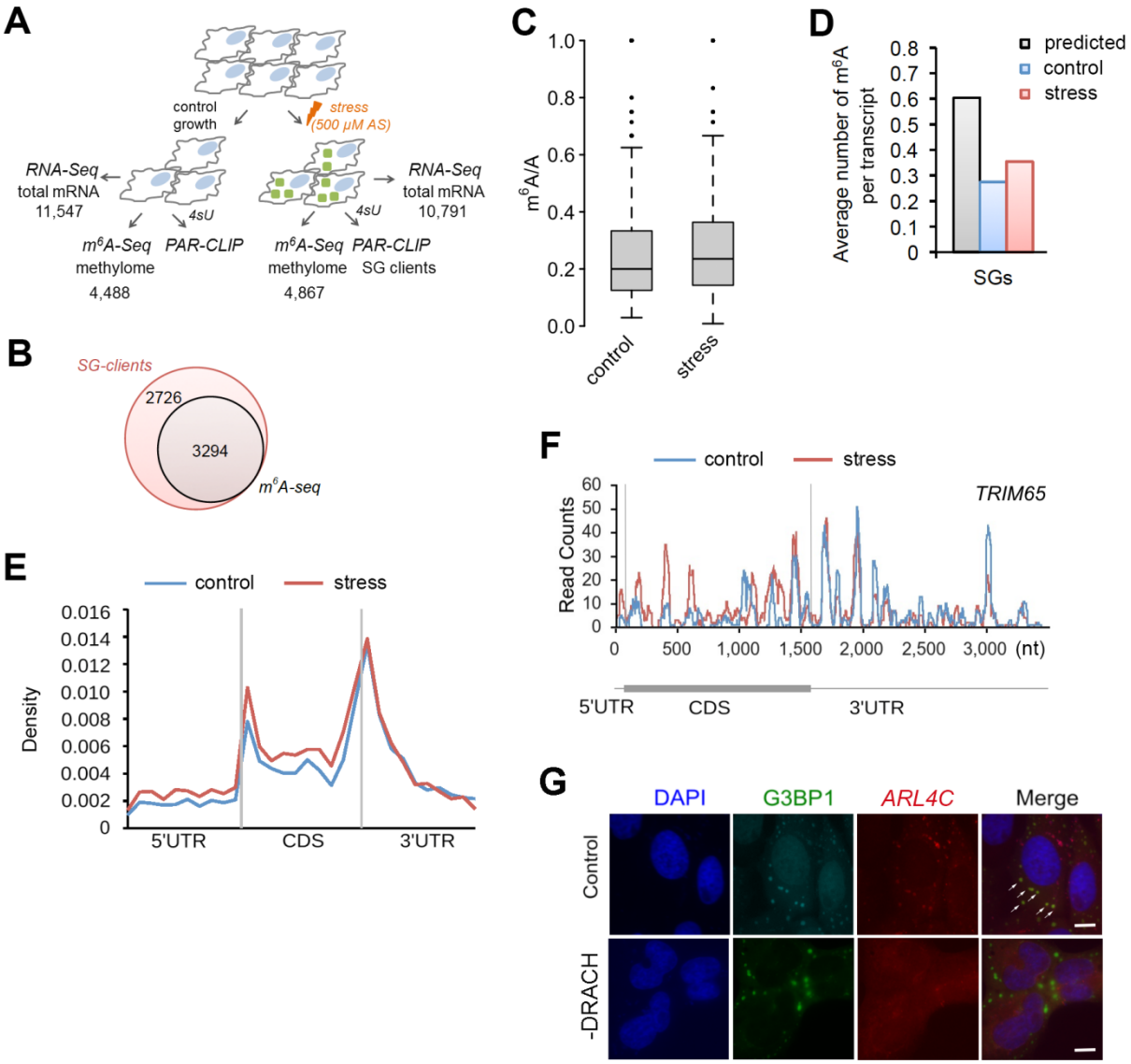

Figure 2 – Site-specific methylation of SG mRNAs in response to oxidative stress
(A) Overview of the experimental set-up. Numbers denote confidently identified mRNAs in each deep-sequencing approach. **(B)** Overlap of the SG transcripts from the PAR-CLIP and m^{6}A-Seq data sets. **(C)** Box-plot of m^{6}A sites (from the m^{6}A-Seq) detected across SG transcripts of untreated HEK-TIA1 cells (control) or exposed to stress (500 µM AS) and presented as a ratio of the total m^{6}A sites (e.g. predicted DRACH motifs designated as A in the ratio m^{6}A/A). p = 5.1x10^{-4} control vs. stress, Mann-Whitney test. **(D)** Average number of m^{6}A modified DRACH motifs detected in the SG mRNAs following stress exposure to 500 µM AS (stress) compared to their methylation level under control growth. p = 1.49x10^{-5} control vs stress, Mann-Whitney test. For comparison the average number of all putative DRACH motifs (predicted) per transcript is also included. **(E)** Metagene profiles of m^{6}A distribution (from the m^{6}A-Seq) along different transcript regions of SG mRNAs from untreated (control) or cells exposed to 500 µM AS (stress). p = 1.4x10^{-3} for 5'UTRs and p = 1.6x10^{-2} for and 5' vicinity of the CDSs; Mann-Whitney test between stress vs. control. Transcript regions were binned for comparable lengths. **(F)** An example of stress-induced m^{6}A modification in the SG transcript *TRIM65*. **(G)** Deletion of the methylation sites in the 5' vicinity of *ARL4C* mRNA hinders its localization into SGs. U2OS-G3BP1 cells expressing ARL4C-CFP with unchanged sequence (control) or deleted DRACH motifs (-DRACH) exposed to 500 µM AS. The colocalization of the wild-type *ARL4C-CFP* mRNA with SGs is designated by

white arrows. *ARL4C-CFP* mRNA was visualized by *in situ* hybridization (FISH). SG (hyperfluorescent loci) were visualized through G3BP1–GFP (green), nuclei were counterstained with DAPI (blue). 58 out 70 cells (83%) showed loss of colocalization by deleted DRACH motifs. Scale bar, 10 µm.

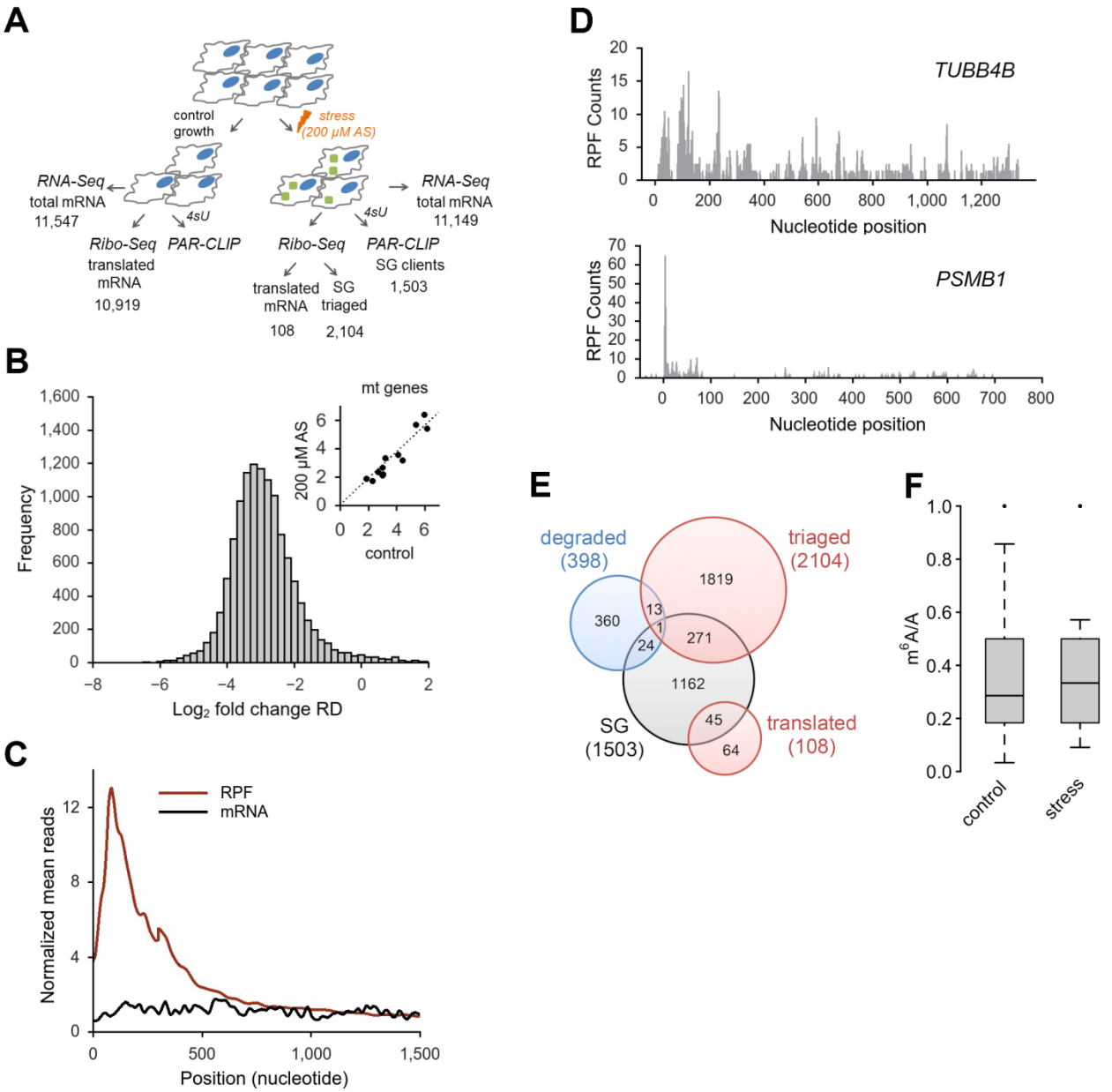

Figure 3 – Oxidative stress globally impairs translation.

(A) Overview of the experimental set-up at mild stress (200 µM AS). Numbers denote confidently identified transcripts in each deep-sequencing approach. **(B)** Log-changes of the ribosome density (RD) values between control and exposed to 200 µM AS HEK-TIA1 cells. Inset, RD values of the mitochondrially-encoded genes which remain unchanged and are used as baseline for normalization of RD values of the nuclearly-encoded genes. **(C)** Cumulative metagene profile of the read density as a function of position for both RPF (from Ribo-Seq) and mRNAs (from RNA-Seq) upon exposure to 200 µM AS. The expressed genes were individually normalized, aligned at the start codon and averaged with equal weight. **(D)** Representative examples of a genuinely translated transcript (*TUBB4B*) and a transcript with stalled translation (*PSMB1*) at 200 µM AS. The first nucleotide of the start codon is designated as zero. **(E)** Venn diagram of the distribution of various transcript groups detected at 200 µM AS. SG, detected in the PAR-CLIP, degraded, identified in the RNA-Seq, red circles, mRNAs with RPFs in the Ribo-Seq. **(F)** Box-plot of m^6A sites (from the m^6A-Seq) detected across the actively translated 108 transcripts in control growth or upon stress exposure and presented as a ratio of the total m^6A sites (e.g. predicted DRACH motifs designated as A in the ratio m^6A/A). p = 0.97 control vs. stress, Mann-Whitney test.

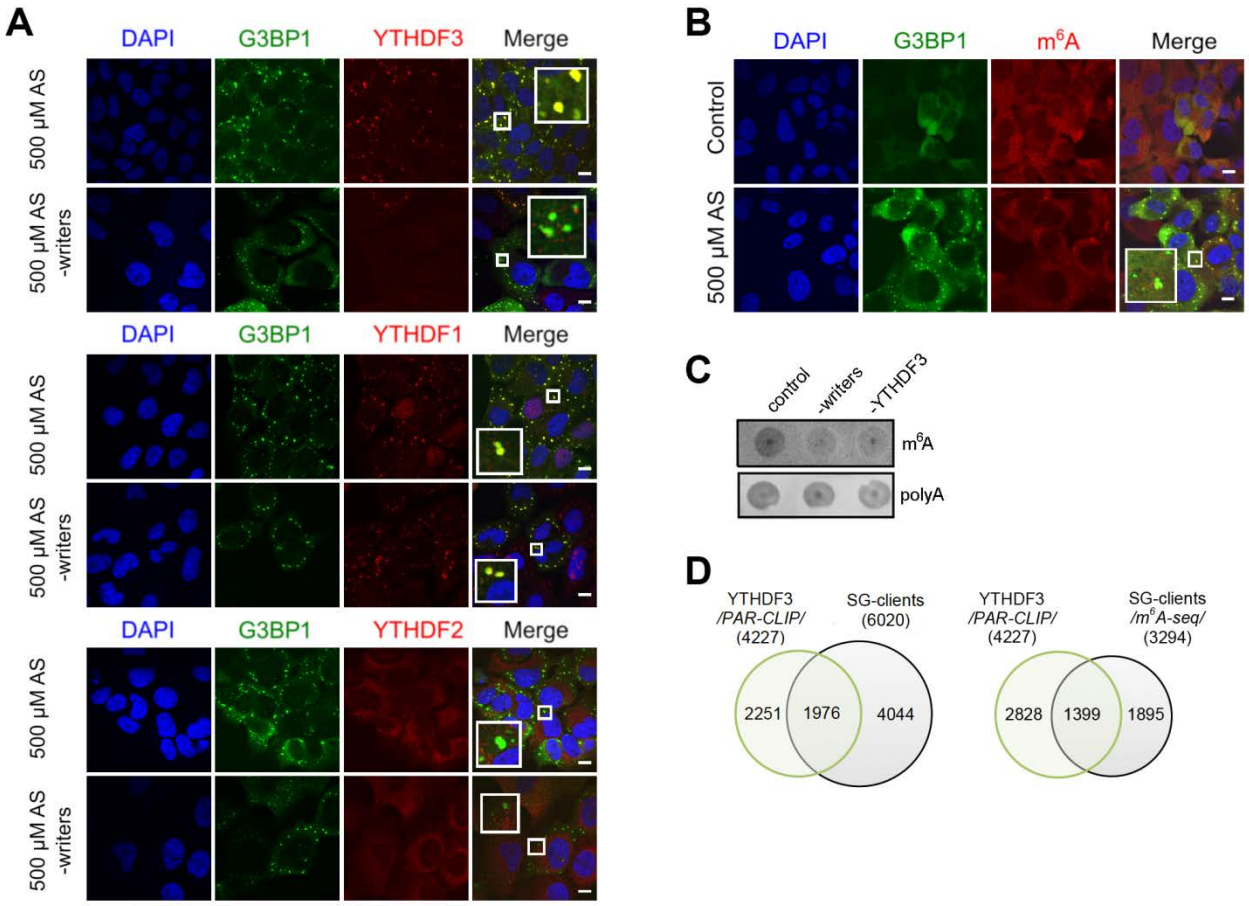

Figure 4 – YDHDF3 colocalizes with m^{6}A-modified mRNA into SGs.
(A) Cellular localization of YTHDF1, YTHDF2 and YTHDF3 in U2OS-G3BP1 cells exposed to oxidative stress (500 µM AS) alone or combined with knockdown (-writers) of the writer complex (*METTL3*, *METTL14* and *WTAP*). Scale bar, 10 µM. **(B)** siRNA knockdown of *YTHDF3* in U2OS-G3BP1 cells abrogated colocalization of m^{6}A-modified RNA within the SGs. **(C)** Total RNA of SGs isolated from U2OS-G3BP1 with siRNA knockdown of the writer complex (-writers) or *YTHDF3* (-YTHDF3), and control cells exposed to 500 µM AS and detected with m^{6}A antibody or fluorescently labeled oligo-dT-primers recognizing the polyA tails of mRNAs. **(D)** Common clients between the YTHDF3 PAR-CLIP target genes (4,227) and total SG clients (6,020 transcripts) and the methylated SG clients detected with high confidence in m^{6}A-Seq (3,294 transcripts). p = $1.07.10^{-155}$ (for PAR-CLIP, left) and p = $3.78.10^{-214}$ (for m^{6}A-Seq, right), hypergeometric test.

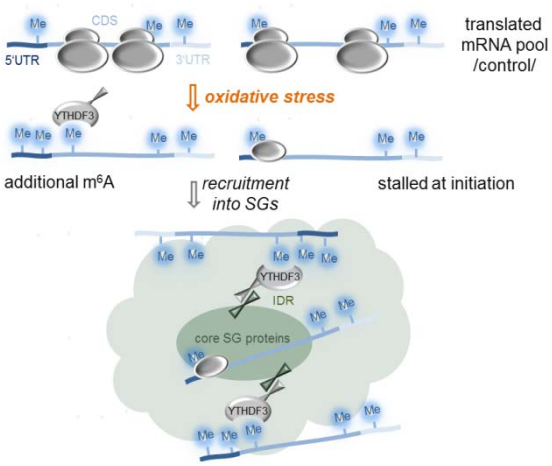

Figure 5 – Proposed model of mRNA triaging into SGs.
mRNAs associate with SGs either by stress-induced methylation in an YTHDF3-dependen manner (left) or by stress-induced stalling at initiation (right). IDR, intrinsically disordered regions.

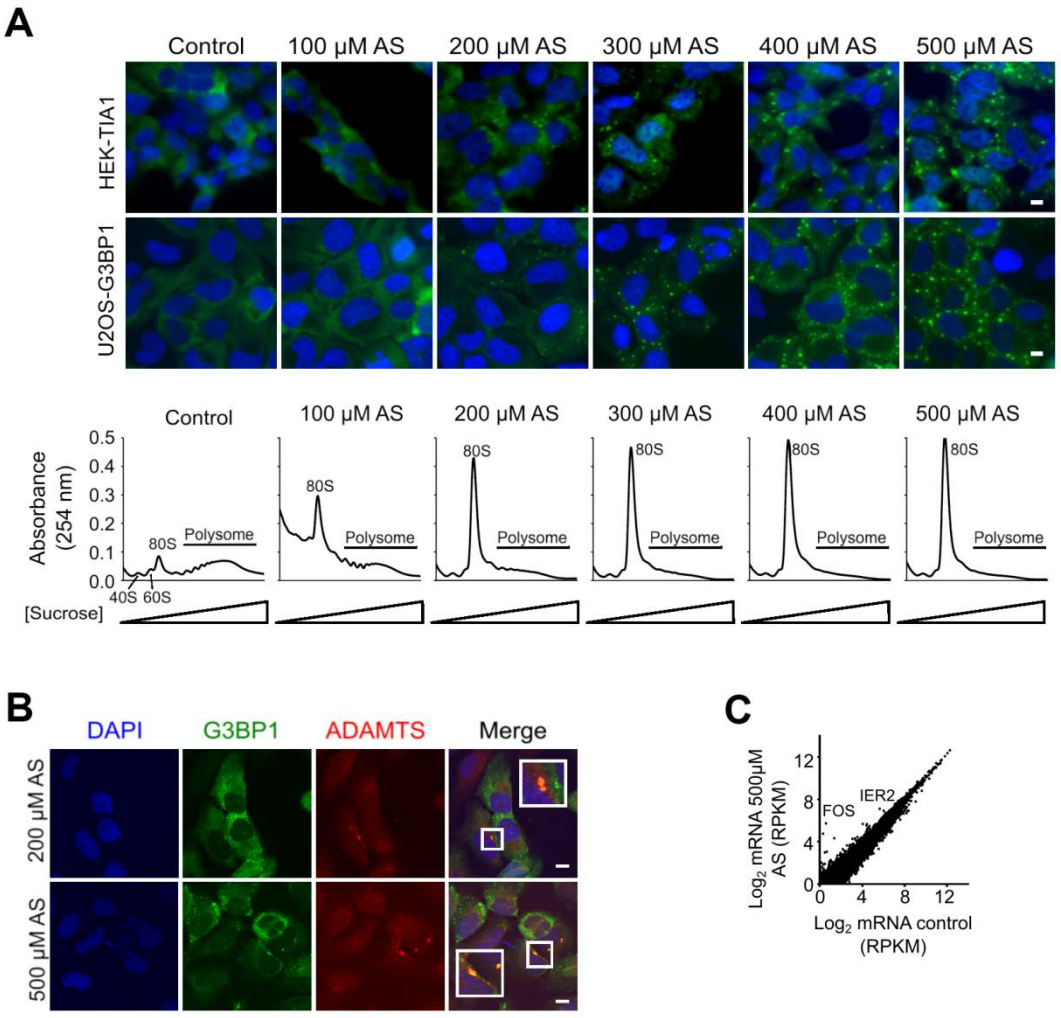

Figure S1 – Exposure to stress and SGs formation.

(A) SG from in concentration-depended manner in U2OS-G3BP1 and HEK-TIA1 cells following exposure to different concentrations of arsenite (AS) for 30 min (upper fluorescent images). TIA1 was visualized with FLAG antibodies (green), G3BP1 – through its fluorescent GFP tag (green), and nuclei were counterstained with DAPI (blue). Control denotes untreated cells. Scale bar, 10 µm. Polysome profiles of HEK-TIA1 cells exposed to different AS concentrations (lower panel). 80S designates an assembled ribosome and 40S and 60S denote the ribosomal subunits. **(B)** mRNAs are sequestered in SGs. *In situ* hybridization (FISH) with combined probe for *ADAMTS1*, *ADAMTS3*, *ADAMTS8*, and *ADAMTS15* transcripts (all also detected as m^6A modified in the m^6A-Seq) in U2OS-G3BP1 exposed for 30 min to AS. Scale bar, 10 µm. **(C)** Comparison between total mRNA from control HEK-TIA1 cells or exposed to 500 µM AS determined from RNA-Seq. Genes with significantly increased expression under stress are designated. R^2= 0.978, Pearson correlation coefficient.

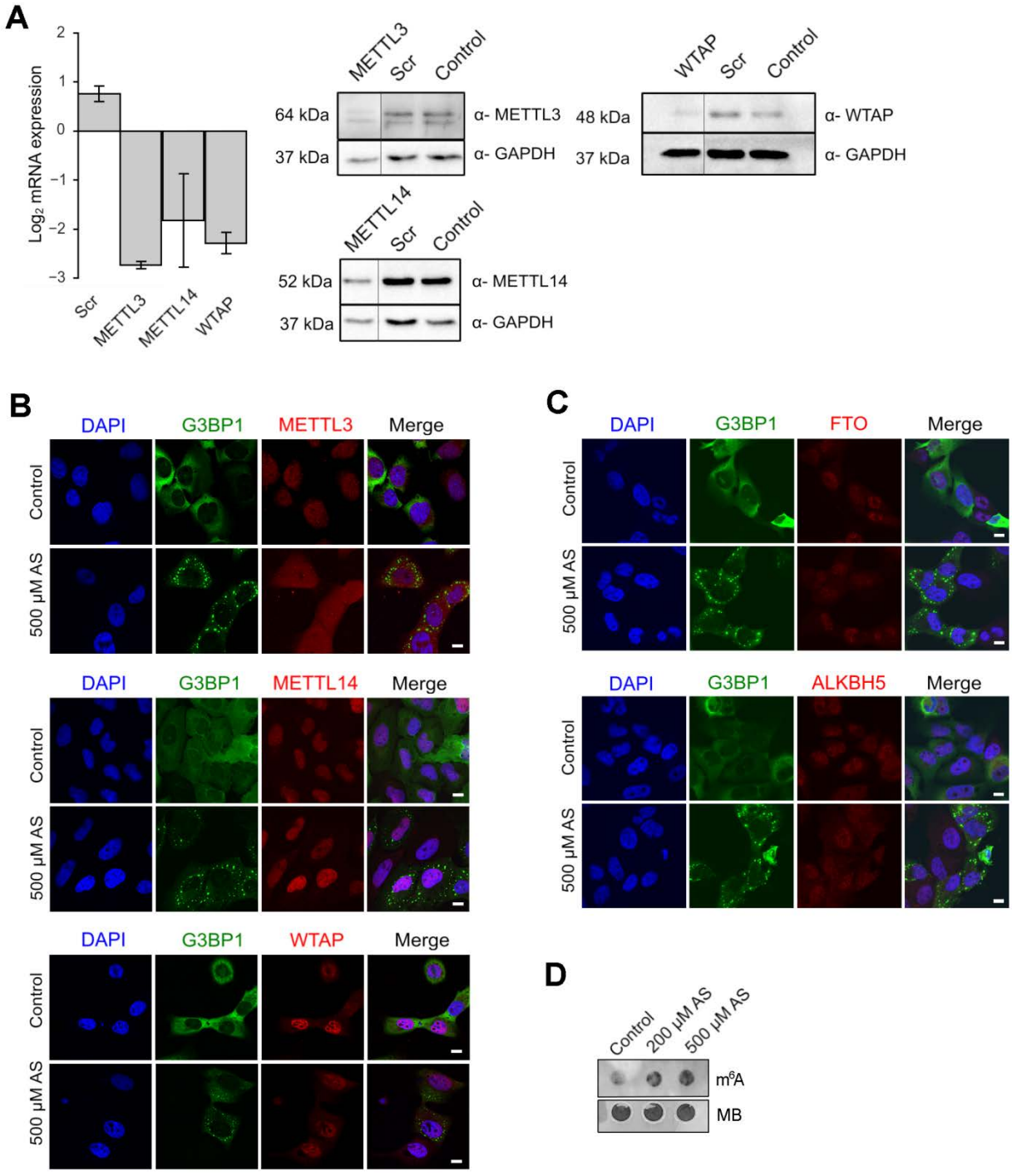

Figure S2 – Cellular localization of the 'writers' and 'erasers' in U2OS-G3BP1 cells.
(A) qRT-PCR following combined siRNA knockdown of the 'writer complex' (*METTL3*, *METTL14* and *WTAP*) for 48h. The levels of each writer mRNA were normalized to the expression of β-actin mRNA. Data are means +/- SD (n = 2). Scr denotes scrambled siRNA and accounts for unspecific effects. Representative Western blots (n = 2) to verify the decrease in the expression of each of the proteins in the writer complex using specific antibodies. GAPDH serves as loading control. **(B)** Localization of METTL3, METTL14 and WTAP under permissive growth and upon stress exposure (500 µM AS, 30 min). G3BP1 detected through its fluorescent GFP tag is used to monitor SG formation under stress. Scale bar, 10 µm.**(C)** Nuclear localization of FTO (upper panel) and ALKH5 (bottom panel) 'erasers' in both control growth and following treatment with 500 µM AS for

30 min. G3BP1 detected through its fluorescent GFP tag is used to monitor SG formation under stress. Scale bar, 10 µm. **(D)** Total RNA isolated from equal amount of HEK-TIA1 cells grown at permissive (control) conditions or exposed to various AS concentrations and detected with m^6A antibody or methylene blue (MB).

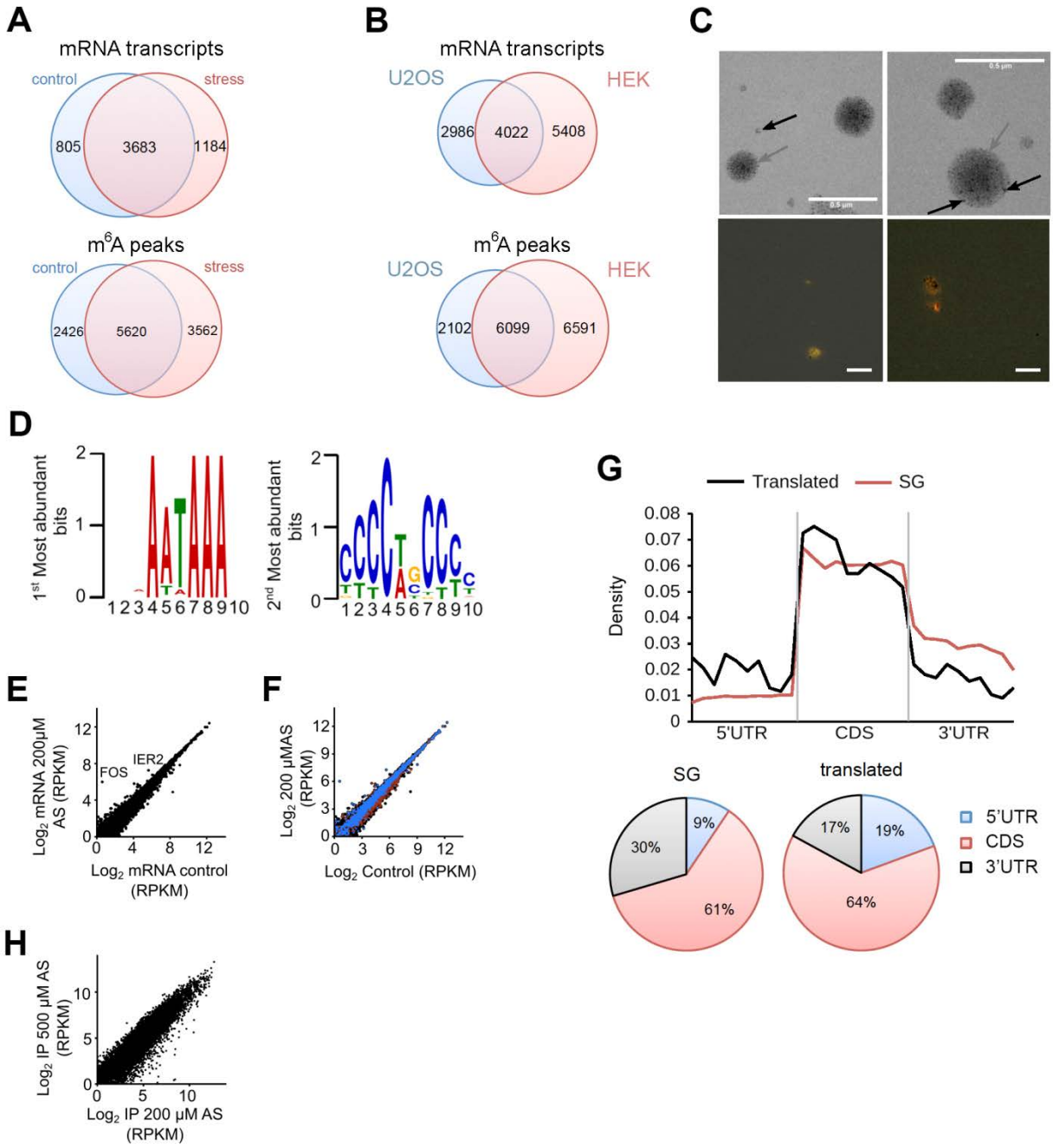

Figure S3 – Analysis of the deep-sequencing data.

(A) Venn diagram of mRNAs containing at least one m^{6}A modification (upper diagram) and m^{6}A peaks detected in mRNAs (lower diagram) identified in HEK-TIA1 (HEK) cells under control growth and at 500 µM AS stress. **(B)** Venn diagram of mRNAs containing at least one m^{6}A modification (upper diagram) and m^{6}A peaks detected in mRNAs (lower diagram) identified in HEK-TIA1 (HEK) cells in this study compared to those in U2OS cells (Xiang et al, 2017). **(C)** Transmission electron microscopy image of isolated SG granules (gray arrow) subjected to PAR-CLIP (upper images). Black arrow indicates magnetic beads (appear as light non-transparent, black dots) used to isolate SGs. FISH on isolated SGs using fluorescently labeled oligo-dT-primers recognizing the polyA tails of mRNAs (red). The yellow/orange color denotes colocalization of polyA-mRNA and G3BP1-GFP (green) signal. Scale bar, 0.5 µM. **(D)** Two most abundant motifs among the SG mRNA clients revealed by MEME motif search. These motifs score for various RNA-binding proteins and not only

for TIA1 (Munteanu et al, 2018). **(E)**. Comparison between total mRNA from control HEK-TIA1 cells or exposed to 200 µM AS determined by RNA-Seq. R^2= 0.992, Pearson correlation coefficient. **(F)** Identified SG clients span a large expression range. Total mRNAs – black, mRNAs in SGs– blue, mRNAs generating RPFs at 200 µM AS – red. **(G)** Distribution of the predicted DRACH motifs (upper plot) or depicted as fractions (lower pie charts) in different transcript segments of the SG clients and translated genes. Transcript regions were binned for comparable lengths. CDS are the longest and exhibit the highest fraction of m^6A motifs. Genes translated under moderate stress exposure (200 µM AS) contain more DRACH motifs in the 5'UTRs compared to the 5'UTRs of the SG mRNA clients, $p = 1.4x10^{-3}$, Mann-Whitney test. **(H)** Correlation of the SG transcripts detected at 200 µM and 500 µM AS in the PAR-CLIP of two merged biological replicates. R^2= 0.883, Pearson correlation coefficient.

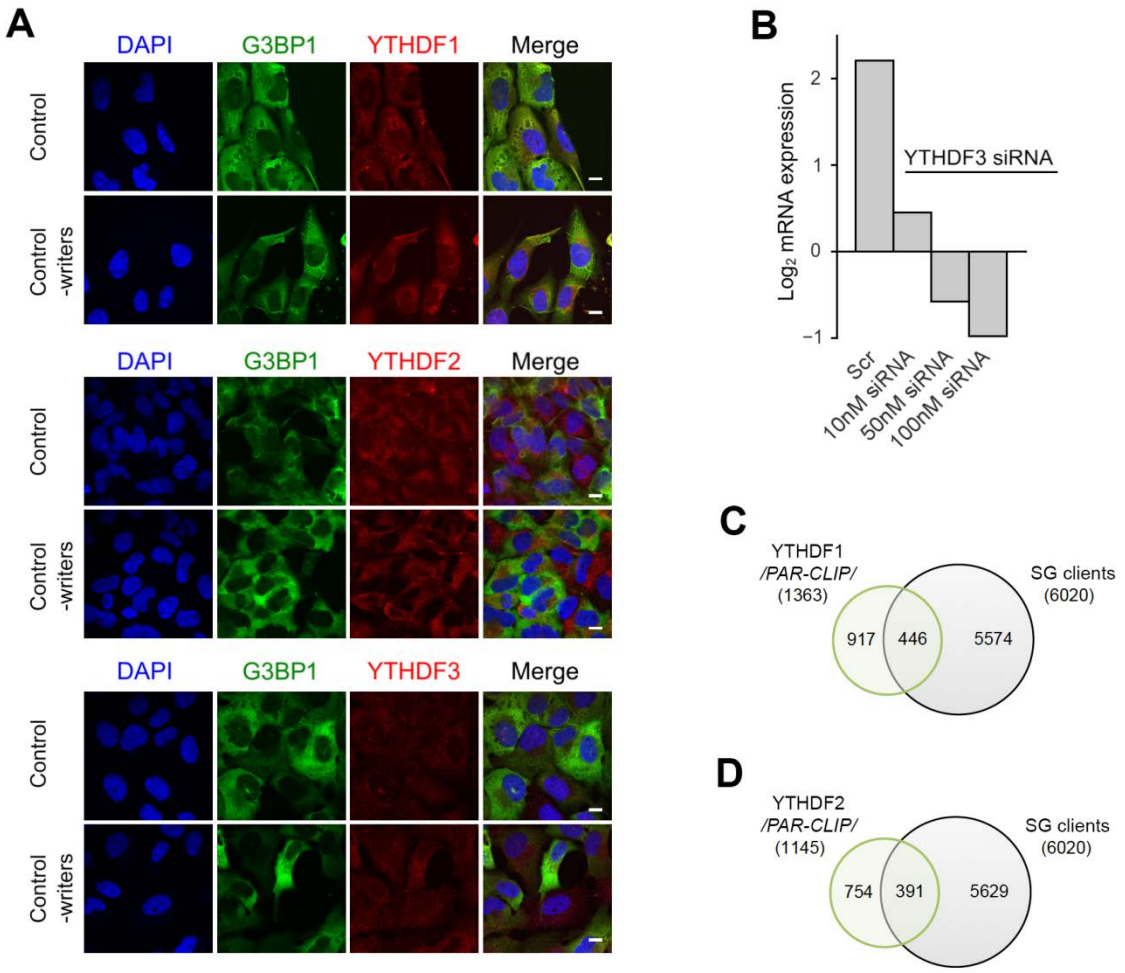

Figure S4 – Localization and clients of the YTHDF readers.

(A) Cytoplasmic localization of YTHDF1, YTHDF2, and YTHDF3 in control, unstressed cells and by silenced 'writers' (*METTL3*, *METTL14* and *WTAP*). The 'readers' were detected with Alexa568-conjugated secondary antibody (red). Scale bar, 10 µm. **(B)** qRT-PCR following siRNA knockdown of *YTHDF3* for 48h in U2OS-G3BP1 cells. The *YTHDF3* expression was normalized to the expression of β-actin mRNA. Scr denotes scrambled siRNA and accounts for unspecific effects. **(C)** mRNA clients of YTHDF1 identified by PAR-CLIP in (Wang et al, 2015) and compared to the SG transcripts identified in this study. p= 0.006, hypergeometric test. **(D)** mRNA clients of YTHDF2 identified by PAR-CLIP in (Wang et al, 2014) and compared to the SG transcripts identified in this study. p= $3.9.10^{-4}$, hypergeometric test.

Table S1. Mass spectrometry identification of SG proteome. Samples from 200 µM and 500 µM AS were independently analyzed for peptide enrichment over non-stressed control. Peptides with spectral counts 1.5-fold greater than non-stressed control in each condition are included and desiganted as Y. Proteins detected in other publications are designated.

Protein name	Gene ID	IP 200 µM AS	IP 500 µM AS	Identified in:
ATP-citrate synthase	ACLY	Y		
Double-stranded RNA-specific adenosine deaminase	ADAR	Y		Ng et al., 2013; Jain et al. 2016
Adenosylhomocysteinase	AHCY	Y		Jain et al, 2016
Allograft inflammatory factor 1-like	AIF1L	Y		
Delta-1-pyrroline-5-carboxylate synthase;Glutamate 5-kinase;Gamma-glutamyl phosphate reductase	ALDH18A1	Y		
Fructose-bisphosphate aldolase A	ALDOA	Y		
AP-1 complex subunit beta-1;AP-2 complex subunit beta	AP1B1;AP2B1	Y		
Sodium/potassium-transporting ATPase subunit alpha-1	ATP1A1	Y		
Ataxin-2	ATXN2	Y	Y	Reviewed in Buchan et al., 2009; Nonhoff et al., 2007; Jain et al. 2016
Ataxin-2-like protein	ATXN2L	Y	Y	Jain et al, 2016
UPF0568 protein C14orf166	C14orf166	Y	Y	Jain et al, 2016
Complement component 1 Q subcomponent-binding protein, mitochondrial	C1QBP	Y	Y	
Calnexin	CANX	Y		
T-complex protein 1 subunit epsilon	CCT5	Y		
T-complex protein 1 subunit zeta	CCT6A	Y		
T-complex protein 1 subunit eta	CCT7	Y		
Creatine kinase B-type	CKB	Y		Jain et al, 2016; Jain et al. 2016
CCR4-NOT transcription complex subunit 1	CNOT1	Y	Y	
CCR4-NOT transcription complex subunit 10	CNOT10	Y	Y	
ATP-dependent RNA helicase DDX3X;ATP-dependent RNA helicase DDX3Y	DDX3X;DDX3Y	Y	Y	Lai et al, 2008; Beckham et al. 2007; Jain et al. 2016

Putative elongation factor 1-alpha-like 3;Elongation factor 1-alpha 1;Elongation factor 1-alpha 2	EEF1A1P5;EEF1	Y		
Elongation factor 2	EEF2	Y		Kimbal et al, 2003
Eukaryotic translation initiation factor 3 subunit A	EIF3A	Y	Y	multisubunit eIF3 reveiwed in Kedersha et al., 2002; Grousl et al. 2009; Jain et al. 2016
Eukaryotic translation initiation factor 3 subunit B	EIF3B		Y	Jain et al, 2016
Eukaryotic translation initiation factor 3 subunit D	EIF3D	Y	Y	Jain et al, 2016
Eukaryotic translation initiation factor 3 subunit E	EIF3E	Y	Y	Jain et al, 2016
Eukaryotic translation initiation factor 3 subunit F	EIF3F		Y	Jain et al, 2016
Eukaryotic translation initiation factor 3 subunit G	EIF3G		Y	Jain et al, 2016
Eukaryotic translation initiation factor 3 subunit H	EIF3H	Y	Y	Jain et al, 2016
Eukaryotic translation initiation factor 3 subunit I	EIF3I	Y	Y	Jain et al, 2016
Eukaryotic translation initiation factor 3 subunit J	EIF3J	Y	Y	Jain et al, 2016
Eukaryotic translation initiation factor 3 subunit K	EIF3K		Y	Jain et al, 2016
Eukaryotic translation initiation factor 3 subunit L	EIF3L	Y		Jain et al, 2016
Eukaryotic initiation factor 4A-I	EIF4A1	Y	Y	Jain et al, 2016
Eukaryotic translation initiation factor 4B	EIF4B	Y		Jain et al, 2016
Eukaryotic translation initiation factor 4 gamma 1	EIF4G1		Y	Reviewed in Buchan et al., 2009; Kedersha et al., 2002; Hoyle et al., 2007; Jain et al, 2016
Eukaryotic translation initiation factor 4 gamma 2	EIF4G2	Y		Reviewed in Buchan et al., 2009; Kedersha et al., 2002; Hoyle et al., 2007; Jain et al. 2016
Eukaryotic translation initiation factor 4 gamma 3	EIF4G3	Y	Y	Kedersha et al., 2002; Hoyle et al., 2007; Jain et al. 2016
Eukaryotic translation initiation factor 5A-1;Eukaryotic translation initiation factor 5A-1-like	EIF5A;EIF5AL1	Y		Reviewed in Buchan et al., 2009; Jain et al. 2016
ELAV-like protein 1	ELAVL1		Y	
Alpha-enolase	ENO1	Y		Jain et al, 2016
Bifunctional glutamate/proline--tRNA ligase;Glutamate--tRNA ligase;Proline--tRNA ligase	EPRS	Y	Y	Reviewed in Buchan et al., 2009; Jain et al. 2016
40S ribosomal protein S30	FAU		Y	Jain et al, 2016

Peptidyl-prolyl cis-trans isomerase FKBP4;Peptidyl-prolyl cis-trans isomerase FKBP4, N-terminally processed	FKBP4	Y		
Fragile X mental retardation protein 1	FMR1		Y	Mazouri et al. 2002;
Far upstream element-binding protein 1	FUBP1	Y	Y	
Far upstream element-binding protein 3	FUBP3		Y	Jain et al, 2016
RNA-binding protein FUS	FUS		Y	Jain et al, 2016
Ras GTPase-activating protein-binding protein 1	G3BP1	Y	Y	Tourriere et al., 2003; Jain et al. 2016
Ras GTPase-activating protein-binding protein 2	G3BP2	Y	Y	Reviewed in Buchan et al., 2009; Jain et al. 2016
Neutral alpha-glucosidase AB	GANAB	Y		Jain et al, 2016
Trifunctional purine biosynthetic protein adenosine-3;Phosphoribosylamine--glycine ligase;Phosphoribosylformylglycinamidine cyclo-ligase;Phosphoribosylglycinamide formyltransferase	GART	Y		Jain et al, 2016
Glucose-6-phosphate isomerase	GPI	Y		
Histidine triad nucleotide-binding protein 1	HINT1	Y		
Histone H3.2;Histone H3.1t;Histone H3.3;Histone H3.1;Histone H3.3C	HIST2H3A;HIST3	Y		
Heterogeneous nuclear ribonucleoprotein A3	HNRNPA3		Y	
Heterogeneous nuclear ribonucleoprotein A/B	HNRNPAB	Y		
Heterogeneous nuclear ribonucleoprotein D0	HNRNPD		Y	Jain et al, 2016
Heterogeneous nuclear ribonucleoprotein D-like	HNRNPDL		Y	Jain et al, 2016
Heterogeneous nuclear ribonucleoprotein F;Heterogeneous nuclear ribonucleoprotein F, N-terminally processed	HNRNPF	Y		Jain et al, 2016
Heterogeneous nuclear ribonucleoprotein U-like protein 2	HNRNPUL2	Y		
Heat shock protein HSP 90-alpha	HSP90AA1	Y		
Endoplasmin	HSP90B1	Y		
60 kDa heat shock protein, mitochondrial	HSPD1	Y		Jain et al, 2016
10 kDa heat shock protein, mitochondrial	HSPE1	Y		Jain et al, 2016
Protein Red	IK	Y	Y	Jain et al, 2016
KH domain-containing, RNA-binding, signal transduction-associated protein 1	KHDRBS1	Y		
Kinesin-1 heavy chain	KIF5B	Y		Jain et al, 2016

L-lactate dehydrogenase A chain	LDHA	Y		Jain et al, 2016
L-lactate dehydrogenase B chain	LDHB	Y		
Leucine-rich PPR motif-containing protein, mitochondrial	LRPPRC	Y		Fujimura et al., 2010; Jain et al. 2016
Leucine-rich repeat-containing protein 47	LRRC47	Y		Jain et al, 2016
Protein LSM12 homolog	LSM12		Y	
Leucine zipper protein 1	LUZP1	Y		
Microtubule-actin cross-linking factor 1, isoforms 1/2/3/5	MACF1	Y		
Microtubule-associated protein 4	MAP4	Y		Jain et al, 2016
Malate dehydrogenase, cytoplasmic	MDH1	Y		
Malate dehydrogenase, mitochondrial	MDH2	Y		Jain et al, 2016
Nucleophosmin	NPM1	Y		
Nuclear migration protein nudC	NUDC	Y		
Nuclear fragile X mental retardation-interacting protein 2	NUFIP2		Y	
Proliferation-associated protein 2G4	PA2G4	Y		
Polyadenylate-binding protein 1	PABPC1		Y	
Polyadenylate-binding protein 4	PABPC4		Y	
Polyadenylate-binding protein 2	PABPN1	Y	Y	Kedersha et al. 1999; Hoyle et al. 2007; Jain et al. 2016
Multifunctional protein ADE2;Phosphoribosylaminoimidazole-succinocarboxamide synthase;Phosphoribosylaminoimidazole carboxylase	PAICS	Y		Jain et al, 2016
Protein deglycase DJ-1	PARK7	Y		
Poly(rC)-binding protein 1	PCBP1		Y	
Poly(rC)-binding protein 2	PCBP2	Y	Y	Fujimura et al., 2008
Protein disulfide-isomerase A3	PDIA3	Y		Reviewed in Buchan et al., 2009; Jain et al. 2016
Phosphatidylethanolamine-binding protein 1;Hippocampal cholinergic neurostimulating peptide	PEBP1	Y		Jain et al, 2016
Retrotransposon-derived protein PEG10	PEG10	Y		
Phosphoglycerate mutase 1;Probable phosphoglycerate mutase 4	PGAM1;PGAM4	Y		
6-phosphogluconate dehydrogenase, decarboxylating	PGD	Y		
Phosphoglycerate kinase 1	PGK1	Y		

Prohibitin	PHB	Y		Ohn et al., 2008
Prohibitin-2	PHB2	Y		
Plastin-3	PLS3	Y		Jain et al, 2016
Polymerase delta-interacting protein 3	POLDIP3		Y	Jain et al, 2016
Peptidyl-prolyl cis-trans isomerase A;Peptidyl-prolyl cis-trans isomerase A, N-terminally processed	PPIA	Y		
Serine/threonine-protein phosphatase 2A 65 kDa regulatory subunit A alpha isoform	PPP2R1A	Y		
Protein PRRC2A	PRRC2A		Y	Jain et al, 2016
Protein PRRC2C	PRRC2C	Y	Y	Jain et al, 2016
Phosphoserine aminotransferase	PSAT1	Y		Jain et al, 2016
26S protease regulatory subunit 7	PSMC2	Y		Jain et al, 2016
Prothymosin alpha;Prothymosin alpha, N-terminally processed;Thymosin alpha-1	PTMA	Y		
Pumilio homolog 1;Pumilio homolog 2	PUM1;PUM2	Y	Y	
RNA-binding protein Raly	RALY		Y	
GTP-binding nuclear protein Ran	RAN	Y		Jain et al, 2016
RNA-binding protein 25	RBM25	Y		Jain et al, 2016
RNA-binding protein 3	RBM3	Y		
RNA-binding motif protein, X chromosome;RNA-binding motif protein, X chromosome, N-terminally processed;RNA binding motif protein, X-linked-like-1	RBMX;RBMXL1		Y	
60S ribosomal protein L13a;Putative 60S ribosomal protein L13a protein RPL13AP3	RPL13A;RPL13A	Y		
60S ribosomal protein L17	RPL17		Y	
40S ribosomal protein S11	RPS11	Y		
40S ribosomal protein S12	RPS12	Y		
40S ribosomal protein S13	RPS13		Y	all proteins of the 40S, Kedersha et al 2002; Grousl et al. 2009; Jain et al. 2016
40S ribosomal protein S14	RPS14	Y		
40S ribosomal protein S15	RPS15	Y		
40S ribosomal protein S2	RPS2	Y		

40S ribosomal protein S21	RPS21	Y	Y	
40S ribosomal protein S24	RPS24		Y	
40S ribosomal protein S28	RPS28	Y		
40S ribosomal protein S5;40S ribosomal protein S5, N-terminally processed	RPS5	Y	Y	
40S ribosomal protein S6	RPS6	Y	Y	
40S ribosomal protein S7	RPS7	Y		
40S ribosomal protein S9	RPS9		Y	
40S ribosomal protein SA	RPSA	Y	Y	
Cell differentiation protein RCD1 homolog	RQCD1	Y	Y	
RuvB-like 1	RUVBL1	Y		
Serine hydroxymethyltransferase, mitochondrial	SHMT2	Y		
Neutral amino acid transporter B(0)	SLC1A5	Y		Jain et al, 2016
Signal recognition particle 14 kDa protein	SRP14	Y		
Double-stranded RNA-binding protein Staufen homolog 1	STAU1		Y	
TAR DNA-binding protein 43	TARDBP	Y	Y	
Threonine--tRNA ligase, cytoplasmic	TARS	Y		Jain et al, 2016
Transcription elongation regulator 1	TCERG1	Y		Jain et al, 2016
T-complex protein 1 subunit alpha	TCP1		Y	
Nucleolysin TIA-1 isoform p40	TIA1	Y	Y	Kedersha et al. 1999; Buchan et al., 2008; Jain et al. 2016
Nucleolysin TIAR	TIAL1		Y	
182 kDa tankyrase-1-binding protein	TNKS1BP1	Y	Y	
Triosephosphate isomerase	TPI1	Y		
Ubiquitin-like modifier-activating enzyme 1	UBA1	Y		Jain et al, 2016
Ubiquitin-associated protein 2-like	UBAP2L	Y		
Ubiquitin carboxyl-terminal hydrolase isozyme L1	UCHL1	Y		Jain et al, 2016
Transitional endoplasmic reticulum ATPase	VCP	Y		Jain et al, 2016
WD repeat-containing protein 1	WDR1	Y		
Tyrosine--tRNA ligase, cytoplasmic;Tyrosine--tRNA ligase, cytoplasmic, N-terminally processed	YARS	Y	Y	Jain et al, 2016

Nuclease-sensitive element-binding protein 1	YBX1		Y	Jain et al, 2016
Y-box-binding protein 3	YBX3		Y	Jain et al, 2016
YTH domain-containing family protein 1	YTHDF1	Y	Y	Jain et al, 2016
YTH domain-containing family protein 2	YTHDF2	Y	Y	Jain et al, 2016
YTH domain-containing family protein 3	YTHDF3	Y	Y	Jain et al, 2016
14-3-3 protein beta/alpha;14-3-3 protein beta/alpha, N-terminally processed	YWHAB	Y		Jain et al, 2016
14-3-3 protein epsilon	YWHAE	Y		Reviewed in Buchan et al., 2009; Jain et al. 2016
Zinc finger CCHC domain-containing protein 3	ZCCHC3		Y	Jain et al, 2016

Beckham, C.J. and Parker, R. P-bodies, stress granules, and viral life cycles. Cell Host Microbe 20, 206-212, (2007).

Buchan, JR, Parker, R, Eukaryotic stress granules: th eins and outs of transaltion, Mol Cell. 25, 932-941 (2009) .

Fujimura, K., Kano, F., and Murata, M. Identification of PCBP2, a facilitator of IRES-mediated translation, as a novel constituent of stress granules and processing bodies. RNA. 14: 425–431, (2008).

Fujimura K, Suzuki T, Yasuda Y, Murata M, Katahira J, Yoneda Y. Identification of importin alpha1 as a novel constituent of RNA stress granules. Biochim. Biphys. Acta 1803, 865-871, (2010).

Grousl, T., Ivanov, P., Frydlova, I., Vasicova, P., Janda, F., Vojtova, J., Malinska, K., Malcova, I., Novakova, L., Janoskova, D. et al. Robust heat shock induces eIF2alpha-phosphorylation-independent assembly of stress granules containing eIF3 and 40S ribosomal subunits in budding yeast, Saccharomyces cerevisiae. J. Cell Sci. 122: 2078–2088, (2009).

Hoyle, N.P., Castelli, L.M., Campbell, S.G., Holmes, L.E., and Ashe, M.P. Stress-dependent relocalization of translationally primed mRNPs to cytoplasmic granules that are kinetically and spatially distinct from P-bodies. J. Cell Biol. 179: 65–74, (2007).

Jain, S., Wheeler, J.R., Walters, R.W., Agrawal, A., Barsic, A., Parker P. ATPase-Modulated Stress Granules Contain a Diverse Proteome and Substructure, Cell 164, 487-498 (2016).

Ng SK, Weissbach R, Ronson GE, Scadden AD. Proteins that contain a functional Z-DNA-binding domain localize to cytoplasmic stress granules. Nucl Acids Res. 41, 9786-9799, (2013).

Nonhoff, U., Ralser, M., Welzel, F., Piccini, I., Balzereit, D., Yaspo, M.L., Lehrach, H., and Krobitsch, S. Ataxin-2 interacts with the DEAD/H-box RNA helciase DDX6 and interferes with P-bodies and stress granules. Mol. Biol. Cell 18: 1385–1396, (2007).

Ohn, T., Kedersha, N., Hickman, T., Tisdale, S., and Anderson, P. A. functional RNAi screen links O-GlcNAc modification of ribosomal proteins to stress granule and processing body assembly. Nat. Cell Biol. 10: 1224–1231, (2008).

Tourrière, H., Chebli, K., Zekri, L., Courselaud, B., Blanchard, J.M., Bertrand, E., and Tazi, J. The RasGAP-associated endoribonucleae G3BP assembles stress granules. J. Cell Biol.160: 823–831, (2003).

Table S2 - List of genes translated under mild oxidative stress (200 µM AS).

		Control growth		Growth at 200 µM AS		Number of DRACH motifs		
Gene ID	Gene name	Total reads mRNA (RPKM)	Total RPF reads (RPKM)	Total reads mRNA (RPKM)	Total RPF reads (RPKM)	5' UTR	CDS	3' UTR
ENSG00000026025	VIM	1213.48	2544.23	1253.46	718.83	0	2	0
ENSG00000063177	RPL18	3961.05	3699.15	4149.19	1284.37	0	2	0
ENSG00000074800	ENO1	4585.25	6285.96	4466.78	1455.00	0	0	0
ENSG00000092841	MYL6	570.46	786.51	622.78	464.66	0	2	0
ENSG00000099800	TIMM13	1094.38	1090.23	1065.98	527.72	0	2	0
ENSG00000100316	RPL3	620.03	1079.95	605.07	501.76	1	2	0
ENSG00000101361	NOP56	668.11	228.33	652.38	138.27	1	2	0
ENSG00000103024	NME3	645.32	421.40	668.66	361.26	0	0	0
ENSG00000103363	TCEB2	780.22	739.43	778.82	279.09	0	1	0
ENSG00000103495	MAZ	983.20	595.25	979.00	345.51	0	3	2
ENSG00000105185	PDCD5	452.10	2296.58	443.92	1480.14	0	0	0
ENSG00000105258	POLR2I	878.61	503.49	882.95	396.59	1	4	0
ENSG00000108518	PFN1	974.96	6247.16	931.90	5812.16	0	1	0
ENSG00000108679	LGALS3BP	335.49	959.04	338.53	392.66	1	5	0
ENSG00000109971	HSPA8	612.88	1726.14	648.41	538.20	0	2	1
ENSG00000111640	GAPDH	1033.85	5809.79	1104.92	1694.83	0	2	1
ENSG00000111669	TPI1	941.05	2312.80	918.16	592.18	0	0	1
ENSG00000111678	C12orf57	421.44	293.75	491.56	180.30	0	0	0
ENSG00000112514	CUTA	302.50	391.56	303.91	288.22	0	0	0
ENSG00000115268	RPS15	391.29	3336.19	472.51	1927.45	0	2	0
ENSG00000122566	HNRNPA2B1	357.50	3288.66	250.00	561.45	0	5	0
ENSG00000125148	MT2A	10.54	148.40	15.83	250.73	0	0	0

ENSG00000125691	RPL23	2203.52	2523.16	2203.49	1260.52	0	1	0
ENSG00000125901	MRPS26	533.34	509.25	546.33	291.92	0	2	1
ENSG00000125995	ROMO1	822.67	918.87	861.04	749.94	0	0	0
ENSG00000126267	COX6B1	2358.85	3490.33	2290.11	2820.98	0	0	1
ENSG00000128272	ATF4	189.67	136.41	216.15	539.91	1	0	0
ENSG00000128626	MRPS12	706.85	541.43	746.36	349.31	1	1	2
ENSG00000130726	TRIM28	904.67	1253.61	888.60	427.83	0	8	0
ENSG00000131469	RPL27	1837.69	2227.03	1838.48	766.10	0	1	0
ENSG00000132341	RAN	656.95	2757.33	666.79	609.61	0	2	1
ENSG00000132475	H3F3B	385.88	1579.28	376.48	716.47	0	1	0
ENSG00000132507	EIF5A	449.46	3664.59	443.16	1461.89	0	1	0
ENSG00000132646	PCNA	676.29	1436.36	639.08	952.12	0	1	0
ENSG00000133124	IRS4	468.64	551.96	298.56	333.18	0	4	0
ENSG00000140990	NDUFB10	824.09	930.40	783.02	388.49	1	3	0
ENSG00000142676	RPL11	2967.41	3509.78	3156.73	1063.05	0	0	0
ENSG00000142937	RPS8	917.80	2553.67	1097.98	860.47	0	0	0
ENSG00000148303	RPL7A	883.84	1230.67	923.43	550.99	0	2	0
ENSG00000149806	FAU	1338.65	2238.70	1389.32	880.84	1	0	0
ENSG00000149925	ALDOA	1573.00	3190.55	1621.33	928.59	3	1	0
ENSG00000150991	UBC	289.60	2966.86	337.10	909.51	1	0	0
ENSG00000156508	EEF1A1	12.23	962.69	20.57	320.43	1	0	1
ENSG00000161016	RPL8	2502.16	3615.94	2627.92	1699.64	1	0	0
ENSG00000161960	EIF4A1	1129.36	432.94	1153.66	316.97	0	3	1
ENSG00000164032	H2AFZ	429.48	1662.91	477.32	658.59	0	0	0
ENSG00000164104	HMGB2	286.74	862.20	262.52	323.92	1	1	0
ENSG00000164898	C7orf55	59.46	97.61	65.48	36.88	0	0	0
ENSG00000166165	CKB	3524.10	6479.33	3994.99	1495.10	1	3	0
ENSG00000166508	MCM7	1274.72	1270.09	1224.78	506.00	1	5	0

ENSG00000166681	NGFRAP1	412.03	635.71	404.45	280.84	0	0	0
ENSG00000167526	RPL13	1010.52	3821.46	1173.45	1719.01	0	2	1
ENSG00000167552	TUBA1A	49.90	1178.24	51.95	313.68	1	2	0
ENSG00000168148	HIST3H3	14.89	82.77	10.99	99.23	0	0	0
ENSG00000168242	HIST1H2BI	53.83	267.58	71.34	229.13	0	0	0
ENSG00000169564	PCBP1	58.10	631.04	58.28	137.14	0	2	0
ENSG00000169710	FASN	239.24	847.90	236.66	288.22	0	21	2
ENSG00000169976	SF3B5	1249.75	1947.65	1380.12	830.17	1	1	2
ENSG00000170043	TRAPPC1	56.08	434.02	52.84	336.98	0	1	0
ENSG00000170315	UBB	714.30	3462.57	809.76	1447.66	0	0	0
ENSG00000171858	RPS21	2110.86	2840.45	2186.55	1673.70	0	2	0
ENSG00000172336	POP7	549.07	378.70	568.36	158.28	2	0	2
ENSG00000173113	TRMT112	347.49	847.82	358.28	381.54	1	1	0
ENSG00000175130	MARCKSL1	292.07	1224.09	262.50	685.19	0	0	1
ENSG00000175334	BANF1	67.91	1219.91	67.89	572.02	1	0	0
ENSG00000175745	NR2F1	23.96	52.80	22.19	23.92	1	2	3
ENSG00000175756	AURKAIP1	863.93	803.39	864.85	326.01	1	1	0
ENSG00000175792	RUVBL1	428.92	412.66	421.99	101.27	0	4	0
ENSG00000176692	FOXC2	0.53	101.07	0.40	368.33	0	6	1
ENSG00000177600	RPLP2	1212.19	2898.76	1318.11	1185.58	0	0	0
ENSG00000177606	JUN	322.87	490.12	550.01	313.70	1	2	1
ENSG00000178952	TUFM	923.87	959.18	981.13	353.33	0	5	0
ENSG00000179010	MRFAP1	291.96	1461.79	284.69	787.16	0	0	2
ENSG00000179029	TMEM107	21.34	16.19	18.44	33.64	0	0	0
ENSG00000179085	DPM3	152.29	289.49	198.30	141.63	1	0	0
ENSG00000182611	HIST1H2AJ	534.45	753.16	565.53	432.79	0	0	0
ENSG00000183011	LSMD1	369.73	305.50	393.65	189.63	2	0	0
ENSG00000183558	HIST2H2AA3	1047.60	2968.33	1042.74	2074.14	0	0	0

ENSG00000183598	HIST2H3D	351.38	2174.61	365.54	1251.21	0	1	0
ENSG00000184009	ACTG1	1840.73	5788.84	1938.13	3329.48	0	2	1
ENSG00000185112	FAM43A	10.73	252.30	8.59	691.41	3	3	0
ENSG00000185787	MORF4L1	31.01	425.79	24.97	187.33	0	1	0
ENSG00000187514	PTMA	230.69	1830.95	218.13	509.80	0	1	0
ENSG00000187634	SAMD11	95.42	41.39	101.98	25.91	0	7	0
ENSG00000188229	TUBB4B	477.61	1857.56	547.02	925.74	0	0	0
ENSG00000188290	HES4	917.66	404.65	933.60	274.18	0	2	0
ENSG00000188620	HMX3	7.39	492.58	5.35	2185.18	2	0	0
ENSG00000189060	H1F0	48.47	128.33	33.71	66.22	1	0	0
ENSG00000196226	HIST1H2BB	12.83	140.76	17.74	150.46	0	0	0
ENSG00000196230	TUBB	587.89	4110.42	585.07	1363.02	0	2	0
ENSG00000196374	HIST1H2BM	10.40	111.61	11.42	80.06	0	0	0
ENSG00000196532	HIST1H3C	3.29	531.80	14.65	303.15	0	0	0
ENSG00000197697	HIST1H2BE	12.40	314.95	26.52	267.22	0	0	0
ENSG00000198374	HIST1H2AL	206.51	1189.00	224.30	685.13	0	0	0
ENSG00000198695	MT-ND6	69.73	680.14	36.61	1891.65	0	0	0
ENSG00000198755	RPL10A	454.27	1343.87	459.83	497.44	0	1	0
ENSG00000204387	C6orf48	261.72	6.24	276.26	41.70	0	0	0
ENSG00000204389	HSPA1A	721.84	3270.28	727.27	1037.21	1	2	0
ENSG00000204628	GNB2L1	5450.96	4344.06	5494.74	1658.72	0	0	0
ENSG00000205155	PSENEN	123.41	303.27	129.39	147.39	0	0	1
ENSG00000212907	MT-ND4L	117.82	441.47	98.93	1360.71	0	0	0
ENSG00000228253	MT-ATP8	51.37	1832.18	19.64	4316.66	0	0	0
ENSG00000233276	GPX1	204.90	207.52	217.61	212.36	2	1	0
ENSG00000233927	RPS28	5.35	1562.77	4.22	1083.66	0	1	3
ENSG00000240972	MIF	1780.88	2867.71	1948.41	1240.01	1	1	1
ENSG00000255302	EID1	16.12	28.18	17.21	27.68	1	0	1

ENSG00000255823	MTRNR2L8	0.34	16.01	0.55	30.33	1	0	0
ENSG00000256618	MTRNR2L1	0.52	21.74	0.76	70.99	1	0	0